HHS Public Access

Author manuscript

J Neurosci Res. Author manuscript; available in PMC 2021 July 01.

Published in final edited form as:

J Neurosci Res. 2021 January ; 99(1): 67–89. doi:10.1002/jnr.24620.

Sex-dimorphic effects of Biogenesis of Lysosome-related Organelles Complex-1 (BLOC-1) deficiency on mouse perinatal brain development

Frank Y. Lee[1], **Jennifer Larimore**[2], **Victor Faundez**[3], **Esteban C. Dell'Angelica**[1], **Cristina A. Ghiani**[4]

[1]Department of Human Genetics, David Geffen School of Medicine, University of California, Los Angeles, California 90095, USA

[2]Department of Biology, Agnes Scott College, Decatur, Georgia 30030, USA

[3]Department of Cell Biology, Emory University, Atlanta, GA 30322, USA

[4]Departments of Pathology & Laboratory Medicine, and Psychiatry & Biobehavioral Sciences, Intellectual and Developmental Disabilities Research Center, David Geffen School of Medicine, University of California Los Angeles, Los Angeles, CA 90095, USA

Abstract

The function(s) of the Biogenesis of Lysosome-related Organelles Complex 1 (BLOC-1) during brain development is hitherto largely unknown. Here, we investigated how its absence alters the trajectory of postnatal brain development using as model the pallid mouse. Most of the defects observed early postnatally in the mutant mice were more prominent in males than in females and in the hippocampus. Male mutant mice, but not females, had smaller brains as compared to sex-matching wild-types at postnatal day 1 (P1), this deficit was largely recovered by P14 and P45. An abnormal cytoarchitecture of the pyramidal cell layer of the hippocampus was observed in P1 pallid male, but not female, or juvenile mice (P45), along with severely decreased expression levels of the radial glial marker GLAST. Transcriptomic analyses showed that the overall response to the lack of functional BLOC-1 was more pronounced in hippocampi at P1 than at P45 or in the cerebral cortex. These observations suggest that absence of BLOC-1 renders males more susceptible to perinatal brain maldevelopment and although most abnormalities appear to have been resolved in juvenile animals, still permanent defects may be present, resulting in faulty

Correspondence to: Cristina A. Ghiani, University of California, Los Angeles (UCLA), Neuroscience Research Building, Suite 375, 635 Charles E Young Drive South, Los Angeles, CA 90095, USA. Cghiani@mednet.ucla.edu.

AUTHOR CONTRIBUTIONS

All authors had full access to all the data in the study and take responsibility for the integrity of the data and the accuracy of the data analysis. *Conceptualization*, C.A.G. and E.C.D.; *Methodology*, F.Y.L. and C.A.G.; *Investigation*, F.Y.L. and C.A.G.; *Formal Analysis*, F.Y.L., E.C.D. and C.A.G.; *Resources*: J.L. and V.F.; *Writing – Original Draft*, F.Y.L. and C.A.G.; *Writing – Review & Editing*, E.C.D. and C.A.G.; *Visualization*, F.Y.L. and C.A.G.; *Supervision*, E.C.D. and C.A.G.; *Funding Acquisition*, E.C.D. and C.A.G.

CONFLICT OF INTEREST

The authors have no conflicting interest to declare.

DATA ACCESSIBILITY

The raw data for the microarrays and the profile plot analyses were deposited in Dryad, University of California Curation Center (UC3), California Digital Library:
https://doi.org/10.5068/D1R67M
Any other raw data will be available upon request.

neuronal circuits, and contribute to previously reported cognitive and behavioural phenotypes in adult BLOC-1-deficient mice.

Graphical Abstract

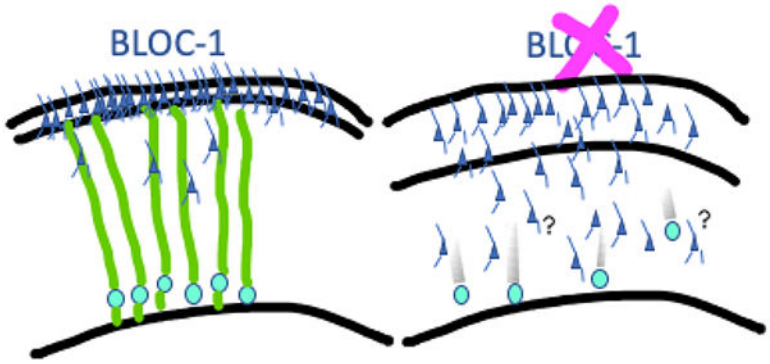

A faulty radial glia scaffold and an abnormal cell layering were observed in the hippocampus of male, but not females, BLOC-1-deficient mice, early postnatally.

Keywords

Pallidin; Dysbindin; Sex differences; Hippocampus; CA1 Pyramidal cell layer; Radial Glia; Process outgrowth

1 | INTRODUCTION

The aetiology of intellectual and developmental disabilities (IDD) is considered to be multifaceted and multifactorial, likely with the contribution of more than one ‘malfunctioning’ gene acting in concert with exogenous/environmental stressors at specific vulnerable developmental windows (Ghiani & Faundez, 2017). Notably, a factor that may greatly influence the susceptibility of an individual to develop a certain neurological syndrome is sex. Several IDD, as well as other psychiatric and neurological disorders, exhibit sex bias in prevalence, age at onset, presentation and severity of symptoms (reviewed by Pinares-Garcia et al., 2019). For example, autism spectrum disorder, attention-deficit hyperactivity disorder, and early-onset schizophrenia (age of onset <20 years) are all diagnosed more often in males than in females (May et al., 2019; Pinares-Garcia et al., 2019). Sex-based differences in comorbidities associated with some IDD have also been documented (Polyak et al., 2015). The underlying causes for such observed sex-based differences are not well understood. Only for very few IDD a genetic basis directly linked to a sex chromosome has been identified, namely Rett Syndrome and Fragile X syndrome caused, respectively, by *de novo* mutations in the *MECP2* gene (Goh, 2017) and repeat expansions in the *FMR1* gene (Hunter et al., 2014), both located on the X chromosome. For most other IDD, the reasons for the documented sex-based differences are likely to be as well multifactorial and complex, including the combinatorial effects of sex hormones and hormone-independent effects of the X and Y chromosomes as modifiers of the disease risk elicited by autosomal gene variants or environmental factors (Green et al., 2019; Pinares-

Garcia et al., 2019). Granted, the study of these effects in humans is quite challenging (Green et al., 2019; May et al., 2019). In mammalian models such as mice, on the other hand, the appropriate modelling of a human neurodevelopmental psychiatric disease represents a major challenge (Sukoff Rizzo & Crawley, 2017) but at least the modifier effects of biological sex on neurodevelopmental alterations caused by autosomal gene mutations should be relatively easier to study, even if these effects were restricted to a specific brain region and/or developmental stage.

In this paper, we report one such example of sex-dimorphic effects of a mutation in an autosomal gene in one particular brain region during perinatal development. The gene in question is *Bloc1s6* (previously known as *Pldn*), which localizes to mouse chromosome 2 and encodes the protein pallidin (Huang et al., 1999). Pallidin and the products of another seven autosomal genes are expressed ubiquitously and assemble into a stable heteromeric complex named Biogenesis of Lysosome-related Organelles Complex (BLOC)-1 (Falcon-Perez et al., 2002; Moriyama & Bonifacino, 2002; reviewed by Ghiani & Dell'Angelica, 2011 and Hartwig et al., 2018). As its name indicates, BLOC-1 was initially studied in the context of the biogenesis of lysosome-related organelles such as melanosomes and platelet dense granules (Falcon-Perez et al., 2002; Moriyama & Bonifacino, 2002). In fact, biallelic loss-of-function mutations in the human pallidin-encoding gene have been shown to cause a rare disease named Hermansky-Pudlak syndrome (HPS) type 9, with the main clinical manifestations arising from defects in lysosome-related organelles such as those already mentioned (Badolato et al., 2012; reviewed by Bowman et al., 2019). On the other hand, interest for investigating potential roles of BLOC-1 in the central nervous system (CNS) arose from the suggestion that common allelic variants in the human *DTNBP1* gene, which encodes the dysbindin subunit of the same complex (Li et al., 2003), might increase the risk for schizophrenia (Straub et al., 2002; Kendler, 2004). Notwithstanding that such proposed association has failed to reach genome-wide statistical significance (Farrell et al., 2015), it stirred an array of studies on possible roles of the dysbindin protein, on its own or as part of BLOC-1, in CNS functions (reviewed by Ghiani & Dell'Angelica, 2011; Mullin et al., 2011; Wang et al., 2017; Hartwig et al., 2018). These studies have led to the recognition that adult mice deficient in BLOC-1, with such deficiency being caused by homozygous mutations in either the dysbindin- or pallidin-encoding genes, display a variety of cognitive and behavioural abnormalities (reviewed by Talbot, 2009; Ghiani & Dell'Angelica, 2011; Mullin et al., 2011; see also Bhardwaj et al., 2015; Spiegel et al., 2015; Petit et al., 2017; Chang et al., 2018; Lee et al., 2018), even when such abnormalities have not been consistently observed among the very few patients reported to suffer from HPS due to mutations in the corresponding human genes (Li et al., 2003; Badolato et al., 2012; Lowe et al., 2013; Yousaf et al., 2016; Bryan et al., 2017; Okamura et al., 2018; Bastida et al., 2019). Interestingly, a small subset of these studies has raised the notion of a putative role for BLOC-1 in mouse brain development. Thus, the levels of both pallidin and dysbindin have been found to be developmentally regulated in the rodent brain (Ghiani et al., 2010; Ito et al., 2010), and lack of BLOC-1 was found to partially impair neurite outgrowth and dendritic spine morphogenesis in vitro (Ghiani et al., 2010; Ito et al., 2010; Ma et al., 2011) as well as neuronal arborization in vivo (Lee et al., 2018).

This study was devoted to investigating how lack of BLOC-1 may impact critical periods of postnatal brain development, specifically, soon after birth, postnatal day (P)1, and during adolescence (P45). Subtle deviations from 'normality' during these windows may trigger permanent functional, behavioural and cognitive deficits, such as those observed in adult BLOC-1-deficient mice. We examined histomorphological abnormalities as well as the expression levels of neural cell markers, including radial glia, in the hippocampus of both male and female mice of the BLOC-1-deficient strain pallid, which is homozygous for a nonsense mutation in the *Bloc1s6* gene. In addition, we investigated the effects of BLOC-1 deficiency on gene expression in the cerebral cortex and hippocampus at both P1 and P45.

2 | MATERIALS AND METHODS

2.1 | Animals

A total of 74 wild-type mice and 82 mutants were used in this study. Male and female mice of the BLOC-1-deficient strain pallid (B6.Cg-*Bloc1s6*^{pa}/J; stock number 000024, The Jackson Laboratory, Bar Harbor, Maine) and of the wild-type control strain C57BL/6J (stock number 000664, The Jackson Laboratory) were from our breeding colony maintained in an approved facility of the Division of Laboratory Animal Medicine at the University of California, Los Angeles (UCLA). The pallid strain is homozygous for a nonsense mutation in the *Bloc1s6* gene encoding pallidin (Huang et al., 1999), an essential component of BLOC-1 (Falcon-Perez et al., 2002; Moriyama and Bonifacino, 2002). The mutation (*Bloc1s6*^{pa}) was originally found in a wild animal (Roberts, 1931) and subsequently backcrossed onto C57BL/6J for 49 generations at The Jackson Laboratory as well as for more than four additional generations in our colony at UCLA. Male mice of the BLOC-1-deficient strain sandy (n=4), which are homozygous for the *Dtnbp1*^{sdy} mutation (Li et al., 2003), and of the control C57BL/6J strain, were from our breeding colony maintained in an approved facility at Emory University. The *Dtnbp1*^{sdy} mutation, which generates an in-frame deletion in all alternatively spliced transcripts encoding dysbindin (Li et al., 2003), was backcrossed onto C57BL/6J for five generations at The Jackson Laboratory and for one additional generation at the University of Pennsylvania (Cox et al., 2009), prior to shipment to our colony at Emory University. Mice were weaned at postnatal day 21 and housed in groups of 2 to 4 based on sex in a temperature- and-light controlled room on a 12-hr light:dark cycle with food (standard chow diet) and water *ad libitum*. Euthanasia prior to tissue dissection of pallid mice (males and females) with their sex- and age-matched controls, and of male sandy mice with age-matched male controls, was performed in accordance to procedures approved by the institutional animal care and use committee at UCLA and Emory University, respectively.

2.2 | Brain wet-weight and body weight measurements

The whole brains of wild-type and pallid mice at P1 (both males and females), as well as at P14 and P45 (only males), were dissected out immediately after euthanasia and rapidly weighted. For some P1 animals, body weight was recorded prior euthanasia. Statistical significance was determined by Two-way ANOVA followed by Bonferroni's multiple comparison test.

2.3 | Histomorphometrical and Immunohistochemical Analyses

P1 male and female, and P45 male, wild-type and pallid mice were anesthetized with isoflurane (30–32%) and transcardially perfused with phosphate-buffered saline (PBS, 0.1 M, pH 7.4) containing 4% (w/v) paraformaldehyde (Electron Microscopy Sciences, Hatfield, PA). The brains were rapidly dissected out, post-fixed overnight in 4% (w/v) paraformaldehyde at 4°C, and cryoprotected in 15% (w/v) sucrose. Coronal sections were cut on a cryostat (Leica, Buffalo Grove, IL) collected sequentially, and paired along the anterior-posterior axis before further processing.

For Nissl Staining, coronal brain sections (20 μm) were stained with a 1% (w/v) cresyl violet (Sigma-Aldrich Corp., St. Louis, MO) solution as previously reported (Lee et al., 2018). Photographs were acquired on a Zeiss Axioskop equipped with a Zeiss colour or monochrome Axiocam using the AxioVision software (Zeiss, Pleasanton, CA) and used to determine the thickness of the cerebral cortex (layers I-VI) in rostral and caudal sections, the outer border and total sectional area of the hippocampus, and the cell density and cytoarchitecture in the Cornu Ammonis (CA)1 subfield of the hippocampus. Measurements were performed by two observers masked to the genotype, sex and age of the animals, from which each histological section has been generated, with the aid of the Zeiss Axiovision or the NIH Image Software (ImageJ, http://rsb.info.nih.gov/ij/). To control and reduce variations due to staining intensity, for the analysis of CA1 cell density, images were acquired using a monochromatic camera (AxioCam; Zeiss). For image analysis of the CA1 cell layer, the “vertical profile plot analysis” feature of ImageJ was used as follows: a grid set at 16,000 square pixels was over-imposed onto each image, and three identical rectangles of height equal to 800 pixels and width equal to 400 pixels (156 μm × 88 μm) were set at a fixed distance from the lateral ventricle (third, fifth, and seventh columns of the grid). The rectangles were positioned such that the long axis would cross completely the pyramidal cell layer, and used to automatically calculate a profile plot as the average pixel intensity per row (i.e., across the short horizontal axis) represented as a function of the position on the long vertical axis. The plots (three plots for each of the left and right hippocampi in each section) were then averaged to obtain one profile per section. To average the profiles of all the sections per animal (8–12 consecutive sections per animal), sixth-order polynomial curves were fitted to each profile per image and used to automatically estimate the mid-point of the cell layer, which in turn was used to align and average the profiles from the different sections to yield one average profile per animal. Data are shown as the mean ± SEM of 4–5 animals per sex, genotype and age.

For Immunohistochemistry, free-floating coronal sections (40 μm) were paired and processed as previously reported (Lee et al., 2018) with minor modifications. Briefly, sections were blocked for 1 h at room temperature in carrier solution [1% (w/v) bovine serum albumin and 0.3% (w/v) Triton X-100] containing 10% (v/v) normal donkey serum, and then incubated for 24 h or 48 h at 4°C with primary antibody (Table 1) diluted in carrier solution containing 5% (v/v) normal donkey serum, followed by the appropriate fluorophore-conjugated secondary antibody (Jackson ImmunoResearch Laboratories, Bar Harbor, ME). Immunostained sections were visualized on a Zeiss Axio Imager 2 equipped

with an AxioCam MRm and the ApoTome imaging system (Zeiss) using either the Axiovision or the Zen software (Zeiss).

2.4 | Proteins and total RNA extractions for Biochemical Analyses

Hippocampi from P1 and P45 wild-type and pallid mice were rapidly dissected, and the two halves frozen separately to be used for protein or total RNA extraction (Ghiani et al., 2010; Lee et al., 2018). For protein extraction, tissue samples were homogenised in lysis buffer [150 mM Tris-HCl, 0.25% (w/v) sodium deoxycholate, 150 mM NaCl, 1 mM EGTA, 1mM EDTA; 1% (w/v) Triton X-100, 0.1% (w/v) SDS, 1 mM sodium vanadate, 1 mM AEBSF, 10 μg/ml Aprotinin, 10 μg/ml Leupeptin, 10 μg/ml pepstatin, and 4 μM sodium fluoride], and clarified by centrifugation at 14,000 rpm for 15 min. The supernatant was collected, and the total protein concentration was estimated using the ThermoScientific™ Pierce™ BCA (bicinchoninic acid) Protein Assay Kit (Waltham, MA). Total RNA was extracted using the Invitrogen™ TRIzol™ reagent (ThermoFisher; Carlsbad, CA) following the manufacturer's protocol from P1 wild-type, pallid and sandy, as well as P45 wild-type and pallid hippocampi. Samples were further purified by treatment with Ambion® TURBO DNA-*free*™ (Life Technologies; Waltham, MA), followed by a second extraction with phenol/chloroform. Sample concentrations and purity were assessed using a ThermoScientific™ NanoDrop™ One Microvolume UV-Vis Spectrophotometer (Canoga Park, CA).

2.5 | Western Blot

Total proteins (35 μg) were resolved on a 4–20% Tris-Glycine gel (Invitrogen, Carlsbad, CA) and then transferred onto PVDF membranes (Bio-Rad Laboratories; Hercules, CA). Equal protein loading was verified first by reversible staining of the blots with Ponceau S solution (Sigma-Aldrich; St. Louis, MO), and later by assessing relative protein levels of β-actin. Membranes were blocked for 1 h at room temperature and incubated overnight with primary antibody (Table 1) diluted in blocking solution [5% (w/v) non-fat milk in PBS containing 0.5% (v/v) Tween-20]. Protein bands were detected by chemiluminescence using the ThermoScientific™ Pierce™ SuperSignal West Pico and/or ECL 2 Western Blotting Substrate or the Amersham ECL kit (GE Healthcare; Piscataway, NJ) with HRP horseradish peroxidase-conjugated secondary antibodies (Cell Signaling; Danvers, MA). Relative intensities of the protein bands were quantified by scanning densitometry using the NIH ImageJ Software. Background-corrected values of each sample were normalised to their respective background-corrected β-actin value. Relative protein levels are expressed as a ratio of the normalised value obtained for each pair of pallid and wild-type hippocampi, which were processed and analysed in parallel, reported as means ± SEM of 4–5 pairs of pallid and wild-type animals per sex, and tested for statistical difference from the theoretical value of 1 by means of one-sample *t* test.

2.6 | Microarray Analysis

Microarray hybridization was performed at the Southern California Genotyping Consortium. Prior to hybridization, the quality of RNA was further monitored using micro-capillary electrophoresis (Bioanalizer 2100, Agilent Technologies; Santa Clara, CA). Total RNA (10 ng/μl) was amplified, labelled, and hybridized to the Illumina MouseRef-8 v2.0 expression array (Illumina; San Diego, CA) overnight at 58°C. The microarrays were then scanned

using an iScan reader, and the signal compiled using BeadStudio software (Illumina). Raw microarray data were analysed using Bioconductor packages and online tools [Database for Annotation, Visualization and Integrated Discovery (DAVID) Bioinformatics Resources, http://david.abcc.ncifcrf.gov/]. Quality assessment was performed by examining the inter-array Pearson correlation and clustering based on the top variant genes. Contrast analysis of differential expression was performed by using the LIMMA (Linear Models for Microarray and RNA-Seq Data) package (Ritchie et al., 2015). After linear model fitting, a Bayesian estimate of differential expression was calculated at a false discovery rate (FDR) of 5% or less. To identify genes with differential expression in P1 hippocampus potentially due to BLOC-1 deficiency, as opposed to strain-specific effects, average mutant-to-wild-type signal ratios (in logarithmic scale base 2) were calculated for each probe yielding a strong signal in at least one genotype (quartile >0.66) in both BLOC-1-deficient mutants pallid and sandy (relative to their matched wild-type controls), and only those probes resulting in a greater than 50% signal increase (logarithm base 2 > 0.6) in both mutants were selected for further analyses. Top enriched biological functions were inferred by means of the Gene Set Enrichment Analysis (GSEA), using the online GEne SeT AnaLysis Toolkit (WebGestalt, http://www.webgestalt.org) and the datasets comprising the relative signals obtained in each BLOC-1-deficient mutant and its wild-type control for all microarray probes yielding relatively strong signals (defined as quartile >0.66 in at least one sample), using standard parameters (5–2000 genes per category, Benjamini-Hochberg procedure to control for multiple comparison).

2.7 | Quantitative Real-Time Polymerase Chain Reaction

Total RNA (600 ng) was reverse-transcribed using the iScript™ cDNA Synthesis Kit (Bio-Rad Laboratories) then analysed for various transcript expressions on a CFX Connect™ Real-Time PCR Detection System (Bio-Rad Laboratories). Reactions were set up using the iQ™ SYBR® Green Supermix (Bio-Rad Laboratories) and the QuantiTect® Primer Assay (Qiagen, Valencia, CA), and performed in triplicate following the manufacturer's directions. Negative controls (samples in which reverse transcriptase was omitted) were amplified individually using the same primer sets to ensure the absence of genomic DNA contamination. Amplification specificity was assessed by melting curve, while standard curves, made from serial dilutions of control RNA, were used for efficiency and quantification. Expression standardization was done using as housekeeping genes *Ppia* (peptidylprolyl isomerase A, also known as cyclophilin A; Gene ID 268373; Mm_Ppia_1_SG QuantiTect Primer Assay, Cat. no. QT00247709) and *Ubc* (ubiquitin C, Gene ID 22190; Mm_Ubc_1_SG QuantiTect Primer Assay, Cat. no. QT00245189). The average values from 3 technical replicates per sample were normalised to those obtained for *Ppia* in the same sample, and the transcript levels in the mutant samples were expressed as means ± SEM relative to the mean value obtained for the wild-type controls. Statistically significant differences were analysed using the Mann-Whitney test.

2.8 | Statistical analyses

Statistical tests for significant differences between groups were performed using Prism 7.0b (GraphPad Software; La Jolla, CA).

3 | RESULTS

3.1 | Decreased brain weight and abnormal organization of the hippocampal pyramidal cell layer in newborn BLOC-1-deficient male mice

Often neurodevelopmental psychiatric disorders exhibit sex bias in the onset, presentation and magnitude of the symptoms, prevalence, although, the influence of genetic heterogeneity and family history, plus the co-morbidity of intellectual and behavioural deficits might also be accountable for such divergencies (Polyak et al., 2015). We examined the impact of lack of BLOC-1 on the gross morphology of the forebrain and its structures early postnatally in both males and females of the mouse strain pallid and congenic wild-type controls. At P1, a difference in brain wet-weight was observed between wild-type male and female mice, with the latter being slighter, on average, however, such difference was absent in the pallid mice. The average wet-weight of freshly dissected brains from pallid males at P1 was about 10% lower as compared to sex- and age-matched wild-types (Figure 1a), such difference reached statistical significance upon two-way ANOVA (Table 2) followed by post-hoc Bonferroni test. Conversely, no differences were observed in the wet-weight of brains from female wild-type and pallid mice at P1 (Figure 1a). To test whether the observed decrease in brain weight could be secondarily due to reduced overall body mass of male pallid mice, both the body weight and the brain-to-body weight ratio were measured in P1 animals. On average, both male and female mutants appeared to be slightly heavier than their sex- and age-matched wild-type controls, although such differences did not reach statistical significance (Figure 1b and Table 2), and, whilst, the brain-to-body weight ratio was lower in mutant mice of both sexes as compared to their corresponding wild-types, only in males, such difference reached statistical significance (Figure 1c and Table 2). Interestingly, the reduction in the overall brain mass observed in male pallid mice at P1 was less apparent as postnatal development progressed to P14 and P45 (Figure 1d and Table 2). These results suggested that BLOC-1 deficiency may differentially affect brain development in mice, depending on sex, prior to or during the perinatal period.

Attempts to test for differences in wet-weight of various brain regions between wild-type and mutant mice at P1 were inconclusive due to significant inter-sample variability in the values obtained. For this practical reason, and because mild abnormalities in cortical or hippocampal structures could potentially underlie some of the behavioural phenotypes reported for BLOC-1-deficient mice (Bhardwaj et al., 2009, 2015; Cox et al., 2009; Ghiani & Dell'Angelica, 2011; Spiegel et al., 2015; Petit et al., 2017; Chang et al., 2018; Lee et al., 2018), we examined the gross anatomical morphology of these two regions in P1 and P45 pallid male mice in comparison to age matched wild-types. The thickness of the cerebral cortex, measured in Nissl-stained rostral and caudal sections from layer I to layer VI, up to the border with the corpus callosum, was not different at P1 between wild-type and pallid mice (Table 3). Likewise, measurements of the cross-sectional area and outer border (perimeter) of the hippocampus exhibited no alterations in the pallid male mice compared to wild-types. Similarly, these brain areas did not show genotypical differences at P45 (Table 3). Despite the lack of gross anatomical deviations, careful examination of the Nissl-stained brain sections revealed an aberrant expansion of the pyramidal cell layer in the hippocampi of male pallid mice at P1 (Figure 2b,d) in comparison to that of hippocampi from sex- and

age-matched controls (Figure 2a,c). In the mutants, the cell bodies were not organised in the typical compact layer of the CA subfields but appeared to be scattered over a large area, with more cell bodies present in the stratum oriens, and a poorly defined separation between the stratum oriens and the pyramidal cell layer (Figure 2a–d). Intriguingly, these abnormalities were more pronounced in pallid males (Figure 2b,d) than in females (Figure 2f), which resembled more closely their wild-type counterpart (Figure 2e). In order to validate these observations using a more objective approach, densitometric analyses were performed on consecutive Nissl-stained sections paired along the anterior-posterior axis, such as those shown in Figure 2. Using a pre-defined grid overlaid on top of the digitally acquired images (Figure 2c–f, blue), three rectangles of identical dimensions were positioned such that the long axis would cross completely the pyramidal cell layer (Figure 2c–f, magenta), and an intensity profile was automatically calculated for each of them as the average pixel intensity per row as a function of the position on the long vertical axis. The resulting profiles were averaged to obtain a single profile per animal. In the case of wild-type mice, the averaged profiles displayed a well-defined peak corresponding to the relatively higher Nissl staining within the pyramidal cell layer; such peak was relatively narrower in P45 males than in P1 males or P1 females (Figure 3a–c, solid black lines). In the case of the pallid mutant mice, the averaged profiles of P1 males looked more like a flat plateau with relatively lower intensity throughout the pyramidal cell layer (Figure 3a), whilst, those of P1 females displayed peaks that were only slightly broader and lower than those of sex- and age-matched wild-types (Figure 3b). The observed abnormal cytoarchitecture was not permanent, and the profiles of P45 males were virtually indistinguishable from those of sex- and age-matched controls (Figure 3c). Hence, absence of functional BLOC-1 in mice hindered the cellular and laminar organization of the hippocampus early postnatally but not at a later developmental stage (P45) that is regarded to as analogous to adolescence (Brust et al., 2015). Importantly, the observed effects were more severe in pallid males, while less prominent or absent in the female counterpart.

3.2 | Lack of BLOC-1 disturbs the radial glia scaffold early postnatally in the hippocampus

Lamination of the cortical regions is required for proper wiring and functioning of the brain, and is achieved through a dynamically coordinated neuronal migration, which comprises multiple cellular and extracellular events (Gupta et al., 2002; Förster et al., 2006; Hayashi et al., 2015). During the first postnatal week, neuronal migration in the rodent hippocampus occurs mostly along a scaffold created by a highly specialised cell type named radial glia (Urban & Guillemot, 2014; Hayashi et al., 2015). We considered the possibility that lack of BLOC-1 might interfere with the formation of the migratory glial scaffold, and examined the expression of a radial glia marker in P1 mutant and wild-type mice. In wild-type mice, strong expression of the Glutamate-Aspartate Transporter (GLAST) was observed in all hippocampal regions (Figure 4a, upper left panel) and well-aligned GLAST-positive processes were visible throughout the pyramidal cell layers (Figure 4a, middle and lower left panels). In contrast, GLAST immunoreactivity was drastically reduced in the whole pallid male hippocampi (Figure 4a, right panels), with fewer positive processes present in the pyramidal cell layer (Figure 4a, right lower panel). This dramatic defect was not observed in hippocampi from pallid females, in which radial glia processes spanned through the cell

layer similarly to sex- and age-matched wild-types (Figure 4b). Consistent with the immunohistochemistry results, immunoblotting analysis of whole-tissue extracts indicated that the steady-state levels of the GLAST protein were reduced by about 36% in hippocampi from pallid males, but not in those from pallid females, as compared to hippocampi from sex- and age-matched wild-type controls (Figure 4c and Table 4). Similarly, processes immunopositive for the intermediate neurofilament nestin were scarce in the pallid male, but not female, hippocampi as compared to sex- and age-matched wild-type controls (Figure 5a,b), a result which was also consistent with determinations of steady-state nestin protein levels by quantitative immunoblotting (Figure 5c and Table 4).

An important factor guiding neuronal migration is the large glycoprotein reelin, secreted by the Cajal-Retzius cells in the marginal zone and known to exist as several isoforms, with the 400-kDa species representing the full-length isoform and the others being the products of proteolytic processing (Ignatova et al., 2004; Jossin et al., 2007). In addition to modulating cell migration by direct binding to receptors on responsive cells, reelin signalling is also important for the development and maintenance of the radial glial scaffold (Förster et al., 2010; Stranahan et al., 2013). Western blot analyses revealed no significant differences in the levels of the three main reelin isoforms (400, 330 and 180 kDa) in P1 mutant males and females as compared to sex- and age-matched wild-types (Figure 6 and Table 4).

We next examined whether the above-described deficits in radial glial scaffold were associated with atypical expression of neuronal markers in P1 mutant hippocampi. The microtubule-associated protein doublecortin is highly expressed in migratory neuroblasts and young neurons, and mutations in the X-linked gene encoding it are associated with aberrant neocortical and hippocampal cellular organisation, epilepsy and severe intellectual disabilities (Corbo et al., 2002; Moon & Wynshaw-Boris, 2013). As judged from immunoblotting analysis, the steady-state expression levels of this protein in hippocampi from male or female pallid mutants did not differ significantly from those of their sex- and age-matched counterparts (Figure 7a and Table 4). Likewise, comparable steady-state protein levels were found between mutant and wild-type mice of both sexes for two immature neuronal markers, α-internexin and βIII-tubulin, (Figure 7a and Table 4). However, an atypical staining pattern for α-internexin was noted in hippocampi from P1 pallid males, particularly near the subiculum (Figure 7b), but not in hippocampi from P1 pallid females (Figure 7c).

These observations suggested that, early postnatally, lack of BLOC-1 results in formation of an aberrant radial glia scaffold and perturbs the perinatal cell layering of the hippocampus in a sex-dependent manner, via a mechanism different from that of canonical players in neuronal migration such as impaired reelin production or processing, or mutations in doublecortin.

3.3 | Upregulated expression of genes promoting tissue development in the hippocampus from male BLOC-1-deficient mice early postnatally

To further investigate the impact of lack of BLOC-1 on brain development in male mice, we examined global mRNA expression in the hippocampus and cerebral cortex from wild-type and pallid animals at P1 and P45. RNA purified from these brain regions was hybridized to

the Illumina MouseRef-8 v2.0 expression array, and the resulting signals were normalised and subjected to statistical analyses to estimate the number of microarray probes detecting transcripts from genes that were expressed in mutant tissue at relatively higher (upregulated) or lower (downregulated) levels, as compared to wild-type controls, at a FDR of less than 5%. As shown schematically in Figure 8a, the number of differentially expressed genes was intriguingly higher in P1 hippocampi than in cerebral cortices at the same age or either brain region at P45. For this reason, subsequent analyses were focused on differential expression of transcripts in the hippocampi of P1 mice.

Given that brain tissue, including the hippocampus, is comprised of more than one cell type, and that significant expansions in cell populations such as macroglial cells are known to occur postnatally (Sauvageot & Stiles, 2002; Silbereis et al., 2016; Zucchero & Barres, 2015), we sought to test whether the observed differences in transcriptome at the tissue level between pallid and wild-type mice at P1 could simply reflect relative changes in cell-type composition, such as abnormally high numbers of macroglial cells at this developmental stage. To this end, we compared the signals obtained for groups of probes in the microarray that targeted transcripts defined by Cahoy et al. (2008) as cell-type-specific markers of neurons, oligodendrocytes and astrocytes, as well as those defined by Zamanian et al. (2012) as markers of reactive astrocytes. For each group of cell-type-specific markers, the average signal intensities resulting from hippocampi of P1 wild-type mice were compared to those from P1 pallid mice. As a reference, similar comparisons were done between wild-type hippocampi at P1 and P45. As expected, the majority of the transcripts defined by Cahoy et al. (2008) as markers of oligodendrocytes and astrocytes were detected at higher levels in hippocampal tissue from wild-type mice at P45 than at P1 (Figure 9, left middle panels, notice the number of data points in the upper-left half of each graph). In contrast, all but two of these transcripts (encoded by *Cldn11* and *Gjb6*, which are markers of oligodendrocytes and astrocytes respectively) were detected at similar levels in hippocampal tissue from wild-type and mutant mice at P1, and so were the groups of transcripts considered as markers of neurons and reactive astrocytes (Figure 9). Although these analyses may not have been sensitive enough to detect or rule out hypothetical alterations in the physiological program of cell proliferation and differentiation in mutant hippocampi, still, they led us to conclude that the changes observed at the transcriptomic level between mutant and wild-type at P1 were unlikely to derive mainly from altered cell composition of the hippocampal tissue.

Strain-specific differences in transcript expression levels in brain have previously been reported for two mouse models of BLOC-1 deficiency, namely sandy and muted (Larimore et al., 2014). In spite of the fact that the strain of pallid mice used for this study is considered congenic with C57BL/6J, still the possibility that some of the differences observed between mutant and control mice at the transcriptomic level might represent strain-specific epiphenomena, instead of a consequence of the lack of BLOC-1 activity, deserved consideration. To address this concern, RNA was isolated from hippocampi dissected from male P1 mice of a second BLOC-1-deficient strain, named sandy (homozygous *Dtnpb1*^{sdy} allele on C57BL/6J background), along with hippocampi form sex- and age-matched wild-type controls housed in the same vivarium, and subjected to microarray analysis under the same conditions used for the samples from pallid mice. The resulting signals (expressed as mutant-to-control ratio) were compared to those obtained for hippocampi from male P1

pallid mice and their corresponding controls. As shown in Figure 8b, the vast majority of probes detected little or no variation in expression levels of their cognate transcripts between each BLOC-1-deficient strain and its corresponding control (log_2 of the mutant-to-control signal ratios ranging between −0.6 and +0.6), while a few detected changes in transcript expression levels in one BLOC-1-deficient strain but not the other. Included in this latter category was a probe detecting the transcript from *Bloc1s6*, which in pallid mice is known to undergo nonsense-mediated mRNA decay (Huang et al., 1999) but is not affected in sandy mice (Figure 8b). Importantly, a small subset of probes detected transcripts that were upregulated by more than 50% (log_2 of mutant-to-control signal ratio >0.6) in both BLOC-1-deficient strains (Figure 8b, upper-right quadrant). As in the case of pallid, analysis of the signals obtained for cell-type-specific markers in hippocampi from sandy mice produced no evidence that the observed changes at the transcriptomic level might be secondary to abnormal cell-type composition in the hippocampus (Figure 9).

Table 5 lists the genes encoding transcripts that were upregulated in hippocampi from both BLOC-1-deficient strains at P1, with the exception of *Dcn*, for which the mutant-to-control signal ratios failed to reach a nominal statistical significance of P<0.05. The transcripts from three of these 31 genes (*Aqp1*, *Folr1* and *Gpc3*) were detected by more than one microarray probe, with comparable results (Table 5). Besides the average mutant-to-control signal ratios obtained for each BLOC-1-deficient strain at P1, the table also provides the mutant-to-control ratios obtained for pallid hippocampi at P45 as well as the average signal ratios between wild-type hippocampi at P45 and P1. It is worth noting that 28 of the 31 genes were not only upregulated in the mutant hippocampi at P1 but also expressed at higher levels in hippocampi from wild-type mice at P45 as compared to hippocampi from wild-type mice at P1 (P45/P1 signal ratio >1.5). In contrast, only the imprinted gene *H19* was found upregulated in mutant hippocampi at P1 and downregulated in wild-type hippocampi at P45. Of note is also the fact that none of the 31 genes upregulated in P1 hippocampi from pallid and sandy mice by more than 50% (mutant-to-control ratio >1.5) were found to be upregulated above the same threshold in hippocampi from pallid mice at P45 as compared to the same tissue from age-matched wild-type controls (Table 5).

The altered expression of seven genes selected from those identified through microarray analyses (Table 5) and known to be upregulated and/or play important roles during brain development was further assessed by qPCR, using hippocampal RNA samples independent from those used for the microarray analyses. Two housekeeping genes, *Ppia* and *Ubc*, which on microarray analysis had yielded mutant-to-control signal ratios of about 1.0, were tested in parallel. As expected, the signals obtained for each of these two housekeeping genes, expressed as Cq values derived from samples containing equal total mRNA content, were virtually indistinguishable when comparing hippocampi from wild-type (n=9) and pallid (n=11) mice at P1 (means ± SEM: *Ppia*, 19.30 ± 0.13 and 19.33 ± 0.13, *Ubc*, 21.00 ± 0.11 and 20.90 ± 0.10, wild-type and pallid samples, respectively), and so were the signals for one of them (*Ubc*) upon normalization to those of the other (*Ppia*) and expressed as an average mutant-to-control ratio (Table 6). One the other hand, the normalised mutant-to-control ratios of transcript expression levels for five of the selected genes (*Aqp1*, *Cldn11*, *Igf2*, *Msx1* and *Ptgds*) were higher than the theoretical value of 1.0 with P<0.05, while those for *Ttr* and *Gpc3* failed to reach statistical significance (Table 6). Thus, a second quantitative

method, using an independent set of samples, allowed validation of some, but not all, of the genes deemed to be upregulated based on microarray analysis of hippocampi from BLOC-1-deficient P1 mice.

Alterations in the expression of genes encoding ion channels (e.g., *Kcne2*) and small-molecule transporters of the SLC superfamily have been previously detected in hippocampi of sandy mice at P7 (Larimore et al., 2017) and were also noted herein in hippocampi from pallid and sandy mice at P1 (Table 5). In addition, other genes listed in Table 5 encode proteins with a wide variety of molecular functions, including but not limited to extracellular growth factors or antagonists (*Igf2, Sostdc1*), transcription factors (*Msx1, Otx2, Zic1*), components or regulators of the extracellular matrix and cell adhesion (*Cldn11, Col6a1, Gjb6, Mgp, Tgfbi*), and metabolism or transport of small signalling molecules (*Enpp2, Ptdgs, Ttr*). In order to test for enrichment of certain biological functions using a more objective approach, GSEA was performed on each set of microarray data comparing hippocampi from P1 pallid or sandy mice with those of matched wild-type controls, and the gene ontology (GO) terms reaching statistical significance at a FDR<0.05 in both datasets were chosen as those most likely to reflect a biological response to BLOC-1 deficiency. This analysis revealed several related biological functions, namely organ development, morphogenesis of branching structures, tissue remodelling and repair, extracellular structure organization, cellular response to growth factors, and protein serine/threonine kinase signalling (Table 7).

Taken together, these findings suggested that lack of BLOC-1 in male mice during perinatal development results in a transcriptomic signature in the hippocampus that is most consistent with an upregulation of mechanisms promoting tissue development. Because such upregulation was no longer apparent in mutant tissue at P45, a later, still highly crucial, time-window of development, it might represent a transient response to an attempt to compensate for some of the observed abnormalities in the development of the hippocampus in the mutants.

4 | DISCUSSION

We had previously shown that BLOC-1 subunits are more abundantly expressed in the mouse brain during perinatal development than in adulthood (Ghiani et al., 2010). In the present work, we provide evidence that lack of functional BLOC-1 not only influenced the trajectory of postnatal brain development but, strikingly, the uncovered defects were more prominent in males than in females, with the hippocampus being the most impacted brain area. Such “mal”-effects were mostly recovered by adolescence, another important window for brain development characterised by profound transformations (Marco et al., 2011; Fuhrmann et al., 2015; Silberies et al., 2016; Herting & Sowell, 2017; Galvan, 2017; Larsen & Luna, 2018), although by the end of this period, young adult (P60) male BLOC-1 deficient mice exhibit alterations in the dentate gyrus and other regions (Lee et al., 2018). These effects were accompanied by absence of GLAST immunopositive processes, and a dramatic decrease in its expression levels. Changes in gene expression were also more evident in the pallid hippocampus at P1.

Our work offers several important points. First, lack of functional BLOC-1 elicits divergent effects in males and females, rendering the former more vulnerable to defects in brain cytoarchitecture. In particular, P1 pallid male brains were found to weight significantly less than those of age- and sex-matching wild-types, while females did not differ from their wild-type counterparts. This phenotype was accompanied by an abnormal organization of the hippocampal pyramidal cell layer, although the expression levels of neuronal markers were unchanged. Sex-associated biochemical and behavioural deficits have been reported for IDD mouse models, but there is scant knowledge on brain cytoarchitecture differences. Genetic variants in catechol-O-methyltransferase (COMT), the enzyme involved in the degradation of catecholamines, have been associated with sex-dependent altered behaviours in both humans and mice. Reduced COMT levels elicited differential effects on the thickness and neuronal density of the cerebral cortex in adult male and female mice, as well as on working memory in both mice and humans (Sannino et al., 2015), which begun to become evident during puberty (Sannino et al., 2017). Curiously, and at variance with humans, both male and female mice carrying mutations in *Mecp2* survive but only the males exhibit neuronal and other Rett syndrome-related phenotypes (Goh, 2017; Jeon et al., 2018). Remarkably, MeCP2 has been shown to regulate the expression levels of BLOC-1 subunits as well as of other interacting proteins, and reduced levels of pallidin were reported in the dentate gyrus of P7 *Mecp2*-null mice (Larimore et al., 2013). Recently, sex-differences in the behaviour of mice null for the main isoform of dysbindin (dysbindin-1A), which display coat colour and prolonged bleeding phenotypes that closely resemble those of the sandy mouse (Petit et al., 2017), have been observed in a series of cognitive and behavioural tests. Whilst the mutant males showed attenuated effects on memory retention in response to acute restrain stress delivered during adolescence (P35), but not during adulthood (P60–70), the females showed lower anxiety (Desbonnet et al., 2019). Male pallid mice showed a high variability in behavioural deficits (Lee et al., 2018). Nonetheless, our findings suggest that, at least at the level of the CNS, male mice are more sensitive than females to the lack of BLOC-1 during critical windows of development.

BLOC-1 deficiency causes HPS, for which only a handful of patients with mutations specifically in this complex are known, and no sex differences on its incidence, presentation or progression are available given the small cohort and variability in the severity of symptoms. In particular, a total of six patients, two males and four females (Li et al., 2003; Lowe et al., 2013; Bryan et al., 2017; Bastida et al., 2019), have been identified as HPS type 7 due to mutations in the *DNTBP1* gene encoding dysbindin. Among them, a 6-year-old boy was diagnosed also with delayed language and motor development (Bryan et al., 2017). The cohort of patients with HPS type 9 due to mutations in the pallidin-encoding gene is even smaller (three females). The first HPS type 9 patient was a 17-year-old female who presented with oculocutaneous albinism, immunodeficiency, and normal neurologic development (Badolato et al., 2012); the second patient was a 4-year-old female with similar symptoms and no reported neurological phenotype (Yousaf et al., 2016). The last patient, a 52-year-old woman, developed schizophrenia in her late forties (Okamura et al., 2018), although the co-occurrence of these two diseases could have just been coincidental.

Second, the maldevelopment was predominantly observed in the hippocampal formation of pallid males during a crucial postnatal time-window and mostly recovered by late

adolescence. This effect was greatly attenuated in pallid females and in the cerebral cortex of either sex, and absent at P45 in pallid males, which had a brain weight and a profile plot practically indistinguishable from their wild-type counterparts. Certain developmental phenotypes have been reported to be more prominent also in the hippocampus of the sandy mice in comparison to the cerebral cortex. Sinclair et al. (2016) showed that the developmental shift in the N-Methyl-D-aspartate receptor (NR) subunits NR2A and NR2B was altered mainly in the hippocampus of sandy males, but not as much in females. Furthermore, developmental deficits in GABAergic neuronal markers and chloride co-transporter expression were found to be greater in the sandy hippocampus than in the cerebral cortex, along with a lower number of parvalbumin interneurons in the CA1 and CA3 of P50 sandy and, to a lesser extent, of P50 mice of another BLOC-1-deficient strain, muted (Larimore et al., 2017). In contrast, albeit not completely unexpected given that mutations in BLOC-1 subunits have been reported to elicit comparable but also divergent phenotypes (Larimore et al., 2014, 2017; Bhardwaj et al 2015; Spiegel et al., 2015; Lee et al., 2018), P50 pallid mice did not show changes in parvalbumin interneurons (Larimore et al., 2017). Accordingly, P1 pallid mice did not present changes in the expression of neuronal markers, despite the fact that these mutants, at P60, exhibited defective dendritic arbours in the dentate gyrus granule cells, but normal in CA1 pyramidal neurones (Lee et al., 2018). The hippocampus is an important hub for cognitive functions as well as memory formation and consolidation, thus the “mal”-effects described could underline the cognitive and behavioural deficits that have been found in both adult pallid and sandy mice (Ghiani & Dell’Angelica, 2011; Spiegel et al., 2015; Lee et al., 2018).

Regardless of the fact that such cytoarchitectural abnormalities were less obvious in the cerebral cortex of pallid males, it cannot be excluded that pallid male mice may display cytoarchitectural abnormalities in other brain regions, which have yet to be fully characterised.

Third, a dramatic absence of radial glia GLAST-positive fibres was observed in the hippocampus of P1 pallid male mice, weakening the migratory scaffold and disturbing the neuronal journey as shown, albeit only perinatally, by the disperse organization of the hippocampal cell layer in pallid male mice compared to their male counterparts. In pallid females, this effect was greatly mitigated, and was resolved in males by P45. BLOC-1 has been shown to be highly expressed in glial cell lineages (Ghiani et al., 2010; Matteucci et al., 2013), hence, it is not surprising that its absence may hamper radial glia functions, along with its involvement in process extension.

Radial glial cells have a bipolar shape with their somata anchored by a short process to the subventricular zone, while a longer one, spanning across the cell layers, attaches to the pial surface along which the immature neurons migrate (Parnavelas & Nadarajah, 2001; Urban & Guillemot, 2014; Hayashi et al., 2015; Xu et al., 2015). BLOC-1-deficient mice presented with an aberrant radial glia scaffold, along with a perturbed cytoarchitectural pattern of the pyramidal cell layer, both in a sex-dependent manner. To better understand the origin of the cell dispersion in the cell layer, we investigated whether signalling from critical players in neuronal migration, e.g. reelin and doublecortin, could be negatively influenced by lack of BLOC-1. Both reelin and doublecortin are required for normal neuronal migration and

consequent brain development, and mutations in the X-linked human genes trigger devastating cortical and hippocampal malformations and disorganisation along with intellectual and behavioural disabilities, and epilepsy. Remarkably, lack of doublecortin has been shown to affect more severely male mice and the hippocampus (Corbo et al., 2002). Since the expression levels of either player were found unchanged, the phenotype observed in P1 pallid male pyramidal cell layer could be primarily attributed to the striking defect in radial glia processes, hence, just be a consequence of the lack of a functional complex and its proposed involvement in process extension. Male pallid mice did not show hippocampal disorganisation by adolescence (P45), still, it will be an overlook not to consider that the proper wiring and formation of the hippocampal neural circuit might be weakened and faulty due to the subtle defects observed, and might underline some of the cognitive and behavioural deficits as those we and others have observed in adult pallid mice, including disrupted sleep and circadian rhythms (Spiegler et al, 2015; Lee et al., 2018). In addition, the reported defective dendritic arbours of the dentate gyrus granule cells in pallid mice would contribute to these deficits (Lee et al., 2018). The dentate gyrus is a hippocampal subregion critical for learning and memory, which receives inputs from the entorhinal cortex and relays them to CA3 for storage. Weak brain wiring may cause altered electrical excitability. Fittingly, the pallid males also displayed abnormal low levels of pCREB/CREB ratio in the hippocampus (Lee et al., 2018), an activity-dependent transcription factor known to be pivotal for cognitive function. Overall these findings strongly highlight that perinatal absence of functional BLOC-1 has repercussions on hippocampal cytoarchitecture and, later in adulthood, function(s). Genetic variants in dysbindin have been associated with altered cognitive functions in humans (reviewed by Hartwig et al., 2018), likely in association with other modifiers.

Fourth, changes in gene expression were again more prominent in the hippocampus of pallid mice at P1 as compared to P45 and to the cerebral cortex at either age. The subtle malformations present in P1 BLOC-1 deficient male mice were largely recovered by adolescence (P45), perhaps, involving some type of compensatory mechanism able to overcome the dysfunction(s) triggered by absence of this complex, and corrected them at some point during the peri-adolescent period. Consistent with this idea, the signature of gene transcripts upregulated in hippocampus from P1 pallid mice was compatible with the biological functions of organ development, morphogenesis of branching structures, tissue remodelling and repair, extracellular structure organization, and cellular response to growth factors.

Altogether these findings indicate that BLOC-1 plays a role during perinatal brain development and seems to be required during this developmental window, at least in the male hippocampus. The alterations described here are subtle and almost resolved by late adolescence, nevertheless, the absence of BLOC-1 during a critical period of brain development may produce long-lasting “mal”-effects, rendering male mice more sensitive and vulnerable to cognitive and behavioural dysfunctions later in life, for instance in adolescence (Marco et al., 2011; Fuhrmann et al., 2015; Galvan, 2017; Larsen & Luna, 2018) and in their response to a stressor. It is worthy to note that ours is one of few reports that documents sex, along with regional, divergent effects in brain anatomy, and places a

special emphasis on the remarkable contribution of sex to the susceptibility to develop IDD in genetically predisposed individual.

Supplementary Material

Refer to Web version on PubMed Central for supplementary material.

ACKNOWLEDGMENTS

The authors would like to thank Drs. Robin S. Fisher and Guido A. Zampighi for their invaluable suggestions and help with the brain morphological analyses; Dr. Giovanni Coppola for his advice and help with the gene arrays data; and Linh Linh Mikutowicz, Diana Nguyen, Chanelle Sy, Christina Falcone, Michaelyn Nguyen, Jaxon Baum, Olivia N Hitchcock, Collette Y Kokikian for their invaluable help with data analyses.

Funding information

Funding was provided by National Institutes of Health grants R01GM112942 and R01GM112942S1 to ECD & CAG; 1R56MH111459 and 1RF1AG060285 to VF. Core equipment used in this study was supported by the Eunice Kennedy Shriver National Institute of Child Health Development under award number: 5U54HD087101.

REFERENCES

Badolato R, Prandini A, Caracciolo S, Colombo F, Tabellini G, Giacomelli M, Cantarini ME, Pession A, Bell CJ, Dinwiddie DL, Miller NA, Hateley SL, Saunders CJ, Zhang L, Schroth GP, Plebani A, Parolini S, & Kingsmore SF (2012). Exome sequencing reveals a pallidin mutation in a Hermansky-Pudlak-like primary immunodeficiency syndrome. Blood, 119, 3185–3187. 10.1182/blood-2012-01-404350 [PubMed: 22461475]

Bhardwaj SK, Baharnoori M, Sharif-Askari B, Kamath A, Williams S, & Srivastava LK (2009). Behavioral characterization of dysbindin-1 deficient sandy mice. Behavioural Brain Research, 197, 435–441. 10.1016/j.bbr.2008.10.011 [PubMed: 18984010]

Bhardwaj SK, Stojkovic K, Kiessling S, Srivastava LK, & Cermakian N (2015). Constant light uncovers behavioral effects of a mutation in the schizophrenia risk gene *Dtnbp1* in mice. Behavioural Brain Research, 284, 58–68. 10.1016/j.bbr.2015.01.048 [PubMed: 25677649]

Bastida JM, Morais S, Palma-Barqueros V, Benito R, Bermejo N, Karkucak M, Trapero-Marugan M, Bohdan N, Pereira M, Marin-Quilez A, Oliveira J, Yucel Y, Santos R, Padilla J, Janusz K, Lau C, Martin-Izquierdo M, Couto E, Francisco Ruiz-Pividal J, Vicente V, Hernández-Rivas JM, González-Porras JR, Luisa Lozano M, Lima M, & Rivera J (2019). Identification of novel variants in ten patients with Hermansky-Pudlak syndrome by high-throughput sequencing. Annals of Medicine, 51, 141–148. 10.1080/07853890.2019.1587498 [PubMed: 30990103]

Bowman SL, Bi-Karchin J, Le L, & Marks MS (2019). The road to lysosome-related organelles: Insights from Hermansky-Pudlak syndrome and other rare diseases. Traffic, 20, 404–435. 10.1111/tra.12646 [PubMed: 30945407]

Bryan MM, Tolman NJ, Simon KL, Huizing M, Hufnagel RB, Brooks BP, Speransky V, Mullikin JC, Gahl WA, Malicdan MCV, & Gochuico BR (2017). Clinical and molecular phenotyping of a child with Hermansky-Pudlak syndrome-7, an uncommon genetic type of HPS. Molecular Genetics and Metabolism, 120, 378–383. 10.1016/j.ymgme.2017.02.007 [PubMed: 28259707]

Brust V, Schindler PM & Lewejohann L (2015). Lifetime development of behavioural phenotype in the house mouse (Mus musculus). Frontiers in Zoology, 12 Suppl 1: S17 10.1186/1742-9994-12-S1-S17 [PubMed: 26816516]

Cahoy JD, Emery B, Kaushal A, Foo LC, Zamanian JL, Christopherson KS, Xing Y, Lubischer JL, Krieg PA, Krupenko SA, Thompson WJ, & Barres BA (2008). A transcriptome database for astrocytes, neurons, and oligodendrocytes: a new resource for understanding brain development and function. Journal of Neuroscience, 28, 264–278. 10.1523/JNEUROSCI.4178-07.2008 [PubMed: 18171944]

Chang EH, Fernando K, Yeung LWE, Barbari K, Chandon TS, & Malhotra AK (2018). Single point mutation on the gene encoding dysbindin results in recognition deficits. Genes Brain and Behavior, 17, e12449 10.1111/gbb.12449

Corbo JC, Deuel TA, Long JM, LaPorte P, Tsai E, Wynshaw-Boris A, & Walsh CA (2002). Doublecortin is required in mice for lamination of the hippocampus but not the neocortex. Journal of Neuroscience, 22, 7548–57. 10.1523/JNEUROSCI.22-17-07548.2002 [PubMed: 12196578]

Cox MM, Tucker AM, Tang J, Talbot K, Richer DC, Yeh L, & Arnold SE (2009). Neurobehavioral abnormalities in the dysbindin-1 mutant, sandy, on a C57BL/6J genetic background. Genes Brain and Behavior, 8, 390–397. 10.1111/j.1601-183X.2009.00477.x

Desbonnet L, O'Tuathaigh CM, O'Leary C, Cox R, Tighe O, Petit EI, Wilson S, & Waddington JL (2019). Acute stress in adolescence vs early adulthood following selective deletion of dysbindin-1A: Effects on anxiety, cognition and other schizophrenia-related phenotypes. Journal of Psychopharmacology, 269881119875465. 10.1177/0269881119875465

Falcón-Pérez JM, Starcevic M, Gautam R, & Dell'Angelica EC (2002). BLOC-1, a novel complex containing the pallidin and muted proteins involved in the biogenesis of melanosomes and platelet-dense granules. Journal of Biological Chemistry, 277, 28191–28199. 10.1074/jbc.M204011200

Farrell MS, Werge T, Sklar P, Owen MJ, Ophoff RA, O'Donovan MC, Corvin A, Cichon S, & Sullivan PF (2015). Evaluating historical candidate genes for schizophrenia. Molecular Psychiatry, 20, 555–562. 10.1038/mp.2015.16 [PubMed: 25754081]

Förster E, Bock HH, Herz J, Chai X, Frotscher M, & Zhao S (2010). Emerging topics in Reelin function. European Journal of Neuroscience, 31, 1511–8. 10.1111/j.1460-9568.2010.07222.x [PubMed: 20525064]

Förster, Zhao, & Frotscher (2006). Laminating the hippocampus. Nature Review Neuroscience, 7, 259–67. https://oii.org10.1038/nrn1882 [PubMed: 16543914]

Fuhrmann D, Knoll LJ, & Blakemore SJ (2015). Adolescence as a Sensitive Period of Brain Development. Trends in Cognitive Science, 19, 558–566. 10.1016/j.tics.2015.07.008

Galvan A (2017). Adolescence, brain maturation and mental health. Nature Neuroscience, 20, 503–504. 10.1038/nn.4530 [PubMed: 28352110]

Ghiani CA, Starcevic M, Rodriguez-Fernandez IA, Nazarian R, Cheli VT, Chan LN, Malvar JS, de Vellis J, Sabatti C, & Dell'Angelica EC (2010). The dysbindin-containing complex (BLOC-1) in brain: developmental regulation, interaction with SNARE proteins and role in neurite outgrowth. Molecular Psychiatry, 15, 204–215. 10.1038/mp.2009.58

Ghiani CA, & Dell'Angelica EC (2011). Dysbindin-containing complexes and their proposed functions in brain: from zero to (too) many in a decade. ASN Neuro, 3, e00058 10.1042/AN20110010 [PubMed: 21504412]

Ghiani CA, & Faundez V (2017). Cellular and molecular mechanisms of neurodevelopmental disorders. Journal of Neuroscience Research, 95, 1093–1096. 10.1002/jnr.24041 [PubMed: 28225560]

Green T, Flash S, & Reiss AL (2019). Sex differences in psychiatric disorders: what we can learn from sex chromosome aneuploidies. Neuropsychopharmacology, 44, 9–21. 10.1038/s41386-018-0153-2 [PubMed: 30127341]

Goh E (2017). Rett syndrome: a sex-biased neurodevelopmental disorder. The Biochemist, 39, 30–33. 10.1042/BIO03901030

Gupta A, Tsai LH, & Wynshaw-Boris A (2002). Life is a journey: a genetic look at neocortical development. Nature Review Genetics, 3, 342–355. 10.1038/nrg799

Hartwig C, Monis WJ, Chen X, Dickman DK, Pazour GJ, & Faundez V (2018). Neurodevelopmental disease mechanisms, primary cilia, and endosomes converge on the BLOC-1 and BORC complexes. Developmental Neurobiology, 78, 311–330. 10.1002/dneu.22542 [PubMed: 28986965]

Hayashi K, Kubo K, Kitazawa A, & Nakajima K (2015). Cellular dynamics of neuronal migration in the hippocampus. Frontiers in Neuroscience, 9, 135 10.3389/fnins.2015.00135 [PubMed: 25964735]

Herting MM, & Sowell ER (2017). Puberty and structural brain development in humans. Frontiers in Neuroendocrinology 44, 122–137. 10.1016/j.yfrne.2016.12.003 [PubMed: 28007528]

Huang L, Kuo YM, & Gitschier J (1999). The pallid gene encodes a novel, syntaxin 13-interacting protein involved in platelet storage pool deficiency. Nature Genetics, 23, 329–332. 10.1038/15507 [PubMed: 10610180]

Hunter J, Rivero-Arias O, Angelov A, Kim E, Fotheringham I, & Leal J (2014). Epidemiology of fragile X syndrome: a systematic review and meta-analysis. American Journal of Medical Genetics Part A, 164A, 1648–1658. 10.1002/ajmg.a.36511 [PubMed: 24700618]

Ignatova N, Sindic CJ, & Goffinet AM (2004). Characterization of the various forms of the Reelin protein in the cerebrospinal fluid of normal subjects and in neurological diseases. Neurobiology of Disease, 15, 326–330. 10.1016/j.nbd.2003.11.008 [PubMed: 15006702]

Ito H, Morishita R, Shinoda T, Iwamoto I, Sudo K, Okamoto K, & Nagata K (2010). Dysbindin-1, WAVE2 and Abi-1 form a complex that regulates dendritic spine formation. Molecular Psychiatry, 15, 976–986. 10.1038/mp.2010.69 [PubMed: 20531346]

Jeon SJ, Gonzales EL, Mabunga DFN, Valencia ST, Kim DG, Kim Y, Adil KJL, Shin D, Park D, & Shin CY (2018). Sex-specific Behavioral Features of Rodent Models of Autism Spectrum Disorder. Experimental Neurobiology, 27, 321–343. 10.5607/en.2018.27.5.321 [PubMed: 30429643]

Jossin Y, Gui L, & Goffinet AM (2007). Processing of Reelin by embryonic neurons is important for function in tissue but not in dissociated cultured neurons. Journal of Neuroscience, 27, 4243–4252. 10.1523/JNEUROSCI.0023-07.2007 [PubMed: 17442808]

Kendler KS (2004). Schizophrenia genetics and dysbindin: a corner turned? American Journal of Psychiatry, 161, 1533–1536. 10.1176/appi.ajp.161.9.1533 [PubMed: 15337639]

Larimore J, Ryder PV, Kim KY, Ambrose LA, Chapleau C, Calfa G, Gross C, Bassell GJ, Pozzo-Miller L, Smith Y, Talbot K, Park IH, & Faundez V (2013). MeCP2 regulates the synaptic expression of a Dysbindin-BLOC-1 network component in mouse brain and human induced pluripotent stem cell-derived neurons. PLoS One, 8, e65069 10.1371/journal.pone.0065069 [PubMed: 23750231]

Larimore J, Zlatic SA, Gokhale A, Tornieri K, Singleton KS, Mullin AP, Tang J, Talbot K, & Faundez V (2014). Mutations in the BLOC-1 subunits dysbindin and muted generate divergent and dosage-dependent phenotypes. Journal of Biological Chemistry, 289, 14291–14300. 10.1074/jbc.M114.553750

Larimore J, Zlatic SA, Arnold M, Singleton KS, Cross R, Rudolph H, Bruegge MV, Sweetman A, Garza C, Whisnant E, & Faundez V (2017). Dysbindin Deficiency Modifies the Expression of GABA Neuron and Ion Permeation Transcripts in the Developing Hippocampus. Frontiers in Genetics, 8, 28 10.3389/fgene.2017.00028 [PubMed: 28344592]

Larsen B, & Luna B (2018). Adolescence as a neurobiological critical period for the development of T higher-order cognition Neuroscience and Biobehavioral Reviews, 94, 179–195 10.1016/j.neubiorev.2018.09.005 [PubMed: 30201220]

Lee FY, Wang HB, Hitchcock ON, Loh DH, Whittaker DS, Kim YS, Aiken A, Kokikian C, Dell'Angelica EC, Colwell CS, & Ghiani CA (2018). Sleep/Wake Disruption in a Mouse Model of BLOC-1 Deficiency. Frontiers in Neuroscience, 12, 759 10.3389/fnins.2018.00759 [PubMed: 30498428]

Li W, Zhang Q, Oiso N, Novak EK, Gautam R, O'Brien EP, Tinsley CL, Blake DJ, Spritz RA, Copeland NG, Jenkins NA, Amato D, Roe BA, Starcevic M, Dell'Angelica EC, Elliott RW, Mishra V, Kingsmore SF, Paylor RE, & Swank RT (2003). Hermansky-Pudlak syndrome type 7 (HPS-7) results from mutant dysbindin, a member of the biogenesis of lysosome-related organelles complex 1 (BLOC-1). Nature Genetics, 35, 84–89. 10.1038/ng1229 [PubMed: 12923531]

Lowe GC, Sánchez Guiu I, Chapman O, Rivera J, Lordkipanidzé M, Dovlatova N, Wilde J, Watson SP, Morgan NV, & UK GAPP collaborative (2013). Microsatellite markers as a rapid approach for autozygosity mapping in Hermansky-Pudlak syndrome: identification of the second HPS7 mutation in a patient presenting late in life. Thrombosis and Haemostasis, 109, 766–768. 10.1160/TH12-11-0876 [PubMed: 23364359]

Ma X, Fei E, Fu C, Ren H, & Wang G (2011). Dysbindin-1, a schizophrenia-related protein, facilitates neurite outgrowth by promoting the transcriptional activity of p53. Molecular Psychiatry, 16, 1105–1116. 10.1038/mp.2011.43 [PubMed: 21502952]

Marco EM, Macrì S, & Laviola G (2011). Critical age windows for neurodevelopmental psychiatric disorders: evidence from animal models. Neurotoxicity Research, 19, 286–307. 10.1007/s12640-010-9205-z [PubMed: 20607469]

Matteucci A, Gaddini L, Macchia G, Varano M, Petrucci TC, Macioce P, Malchiodi-Albedi F, & Ceccarini M (2013). Developmental expression of dysbindin in Muller cells of rat retina. Experimental Eye Research, 116, 1–8. 10.1016/j.exer.2013.08.006 [PubMed: 23954924]

May T, Adesina I, McGillivray J, & Rinehart NJ (2019). Sex differences in neurodevelopmental disorders. Current Opinion in Neurology, 32, 622–626. 10.1097/WCO.0000000000000714 [PubMed: 31135460]

Moriyama K, & Bonifacino JS (2002). Pallidin is a component of a multi-protein complex involved in the biogenesis of lysosome-related organelles. Traffic, 3, 666–677. 10.1034/j.1600-0854.2002.30908.x [PubMed: 12191018]

Moon HM, & Wynshaw-Boris A (2013). Cytoskeleton in action: lissencephaly, a neuronal migration disorder. WIREs Developmental Biology, 2, 229–245. 10.1002/wdev.67 [PubMed: 23495356]

Mullin AP, Gokhale A, Larimore J, & Faundez V (2011). Cell biology of the BLOC-1 complex subunit dysbindin, a schizophrenia susceptibility gene. Molecular Neurobiology, 44, 53–64. 10.1007/s12035-011-8183-3 [PubMed: 21520000]

Okamura K, Abe Y, Araki Y, Wakamatsu K, Seishima M, Umetsu T, Kato A, Kawaguchi M, Hayashi M, Hozumi Y, & Suzuki T (2018). Characterization of melanosomes and melanin in Japanese patients with Hermansky-Pudlak syndrome types 1, 4, 6, and 9. Pigment Cell & Melanoma Research, 31, 267–276. 10.1111/pcmr.12662 [PubMed: 29054114]

Parnavelas JG, & Nadarajah B (2001). Radial Glial Cells: Are They Really Glia? Neuron, 31, 881–884. 10.1016/S0896-6273(01)00437-8 [PubMed: 11580889]

Petit EI, Michalak Z, Cox R, O'Tuathaigh CM, Clarke N, Tighe O, Talbot K, Blake D, Joel J, Shaw A, Sheardown SA, Morrison AD, Wilson S, Shapland EM, Henshall DC, Kew JN, Kirby BP, & Waddington JL (2017). Dysregulation of Specialized Delay/Interference-Dependent Working Memory Following Loss of Dysbindin-1A in Schizophrenia-Related Phenotypes. Neuropsychopharmacology, 42, 1349–1360. 10.1038/npp.2016.282 [PubMed: 27986973]

Pinares-Garcia P, Stratikopoulos M, Zagato A, Loke H, & Lee J (2019). Sex: A Significant Risk Factor for Neurodevelopmental and Neurodegenerative Disorders. Brain Sciences, 8, E154 10.3390/brainsci8080154

Polyak A, Rosenfeld JA, & Girirajan S (2015). An assessment of sex bias in neurodevelopmental disorders. Genome Medicine, 7, 94 10.1186/s13073-015-0216-5 [PubMed: 26307204]

Ritchie ME, Phipson B, Wu D, Hu Y, Law CW, Shi W, & Smyth GK (2015). *limma* powers differential expression analyses for RNA-sequencing and microarray studies. Nucleic Acids Research, 43, e47 10.1093/nar/gkv007 [PubMed: 25605792]

Roberts E (1931). A new mutation in the house mouse (Mus musculus). Science, 74, 569 10.1126/science.74.1927.569

Sannino S, Gozzi A, Cerasa A, Piras F, Scheggia D, Managò F, Damiano M, Galbusera A, Erickson LC, De Pietri Tonelli D, Bifone A, Tsaftaris SA, Caltagirone C, Weinberger DR, Spalletta G, & Papaleo F (2015). COMT Genetic Reduction Produces Sexually Divergent Effects on Cortical Anatomy and Working Memory in Mice and Humans. Cerebral Cortex, 25, 2529–41. 10.1093/cercor/bhu053 [PubMed: 24658585]

Sannino S, Padula MC, Managò F, Schaer M, Schneider M, Armando M, Scariati E, Sloan-Bena F, Mereu M, Pontillo M, Vicari S, Contarini G, Chiabrera C, Pagani M, Gozzi A, Eliez S, & Papaleo F (2017). Adolescence is the starting point of sex-dichotomous COMT genetic effects. Translational Psychiatry, 7, e1141 10.1038/tp.2017.109 [PubMed: 28556830]

Sauvageot CM & Stiles CD (2002). Molecular mechanisms controlling cortical gliogenesis. Current Opinion in Neurobiology, 12, 244–249. 10.1016/S0959-4388(02)00322-7 [PubMed: 12049929]

Silbereis JC, Pochareddy S, Zhu Y, Li M, & Sestan N (2016). The Cellular and Molecular Landscapes of the Developing Human Central Nervous System. Neuron, 89, 248–268. 10.1016/j.neuron.2015.12.008 [PubMed: 26796689]

Sinclair D, Cesare J, McMullen M, Carlson GC, Hahn CG, & Borgmann-Winter KE (2016). Effects of sex and DTNBP1 (dysbindin) null gene mutation on the developmental GluN2B GluN2A switch

in the mouse cortex and hippocampus. Journal of Neurodevelopmental Disorders, 8, 14 10.1186/s11689-016-9148-7 [PubMed: 27134685]

Spiegel S, Chiu A, James AS, Jentsch JD, & Karlsgodt KH (2015). Recognition deficits in mice carrying mutations of genes encoding BLOC-1 subunits pallidin or dysbindin. Genes Brain and Behavior, 14, 618–624. 10.1111/gbb.12240

Sukoff Rizzo SJ, & Crawley JN (2017). Behavioral Phenotyping Assays for Genetic Mouse Models of Neurodevelopmental, Neurodegenerative, and Psychiatric Disorders. Annual Review of Animal Biosciences, 5, 371–389. 10.1146/annurev-animal-022516-022754 [PubMed: 28199172]

Stranahan AM, Erion JR, & Wosiski-Kuhn M (2013). Reelin signaling in development, maintenance, and plasticity of neural networks. Ageing Research Reviews, 12, 815–22. 10.1016/j.arr.2013.01.005 [PubMed: 23352928]

Straub RE, Jiang Y, MacLean CJ, Ma Y, Webb BT, Myakishev MV, Harris-Kerr C, Wormley B, Sadek H, Kadambi B, Cesare AJ, Gibberman A, Wang X, O'Neill FA, Walsh D, & Kendler KS (2002). Genetic variation in the 6p22.3 gene *DTNBP1*, the human ortholog of the mouse dysbindin gene, is associated with schizophrenia. American Journal of Human Genetics, 71, 337–348. 10.1086/341750 [PubMed: 12098102]

Talbot K (2009). The sandy (sdy) mouse: a dysbindin-1 mutant relevant to schizophrenia research. Progress in Brain Research, 179, 87–94. 10.1016/S0079-6123(09)17910-4 [PubMed: 20302821]

Urbán N & Guillemot F (2014). Neurogenesis in the embryonic and adult brain: same regulators, different roles. Frontiers in Cellular Neuroscience, 8, 396 10.3389/fncel.2014.00396 [PubMed: 25505873]

Wang H, Xu J, Lazarovici P, & Zheng W (2017). Dysbindin-1 Involvement in the Etiology of Schizophrenia. International Journal of Molecular Science, 18, E2044 10.3390/ijms18102044

Yousaf S, Shahzad M, Kausar T, Sheikh SA, Tariq N, Shabbir AS University of Washington Center for Mendelian Genomics, Ali M, Waryah AM, Shaikh RS, Riazuddin S, & Ahmed ZM (2016). Identification and clinical characterization of Hermansky-Pudlak syndrome alleles in the Pakistani population. Pigment Cell & Melanoma Research, 29, 231–235. 10.1111/pcmr.12438 [PubMed: 26575419]

Xu L, Tang X, Wang Y, Xu H, & Fan X (2015). Radial glia, the keystone of the development of the hippocampal dentate gyrus. Molecular Neurobiology, 51, 131–41. 10.1007/s12035-014-8692-y [PubMed: 24719081]

Zamanian JL, Xu L, Foo LC, Nouri N, Zhou L, Giffard RG, & Barres BA (2012). Genomic analysis of reactive astrogliosis. Journal of Neuroscience, 32, 6391–6410. 10.1523/JNEUROSCI.6221-11.2012 [PubMed: 22553043]

Zuchero JB & Barres BA (2015). Glia in mammalian development and disease. Development, 142, 3805–3809. https://doi:10.1242/dev.129304 [PubMed: 26577203]

Significance

Sex is a decisive factor involved in shaping brain functions across life, albeit often ignored when it comes to investigation in models of intellectual and developmental disabilities (IDD). Early postnatal brain development is a critical window sensitive to genetic and environmental challenges, which will shape its functionality and may cause life-long cognitive and behavioural disabilities. Our study documents sex, along with regional, divergent effects in brain anatomy caused by a single mutation in an autosomal gene, and places a special emphasis on the remarkable contribution of sex to the susceptibility to develop IDD in genetically predisposed individuals.

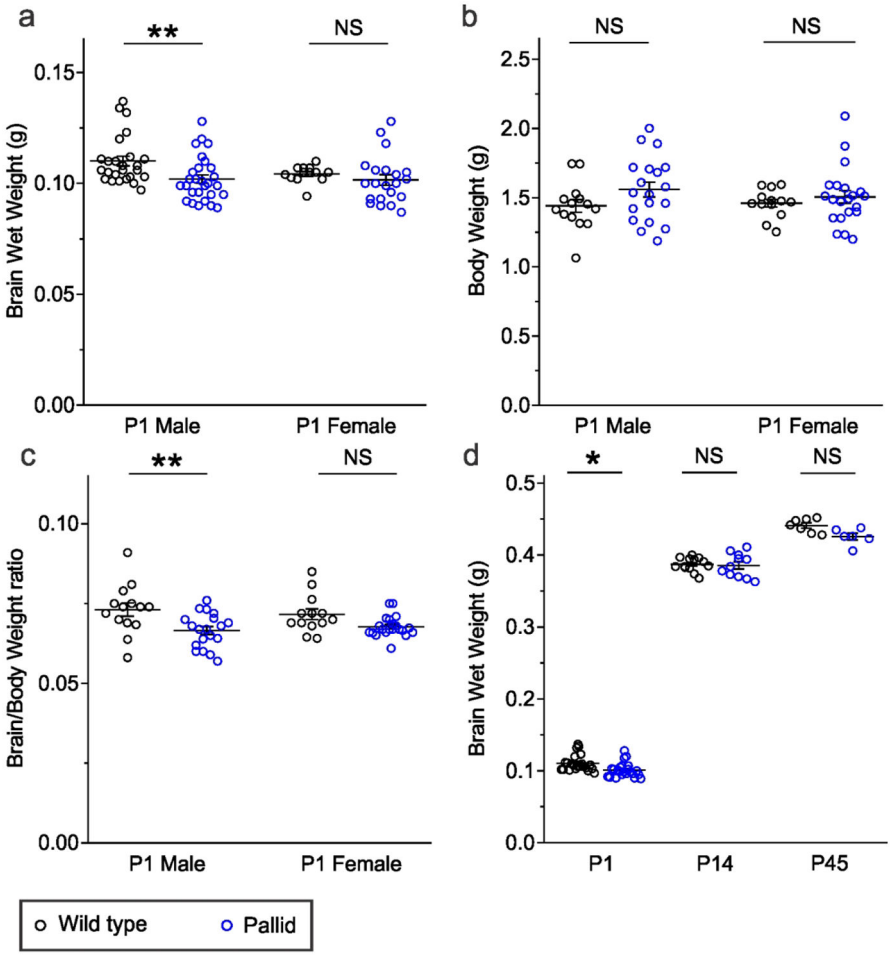

FIGURE 1.

Decreased brain weight in BLOC-1-deficient male mice at postnatal day 1. (a) Wet weight of freshly dissected whole brains, (b) whole body weight, and (c) brain-to-body weight ratio were determined in both males and females of the C57BL/6J strain (wild-type) and the congenic BLOC-1-deficient strain pallid, at postnatal day (P) one (P1). (d) Wet weight of freshly dissected whole brains from male mice of the wild-type and pallid strains at P1, P14 and P45. In (a) through (d), each small circle represents the value obtained from one animal, the wide horizontal lines represent arithmetic mean values, and the error bars represent SEM. The numbers of animals for each group are listed in Table 2. Statistical analyses were performed using two-way Analysis of variance (see Table 2) followed by Bonferroni comparisons of selected group pairs: NS, non-significant; *p<0.05; **p<0.01; ****p<0.0001.

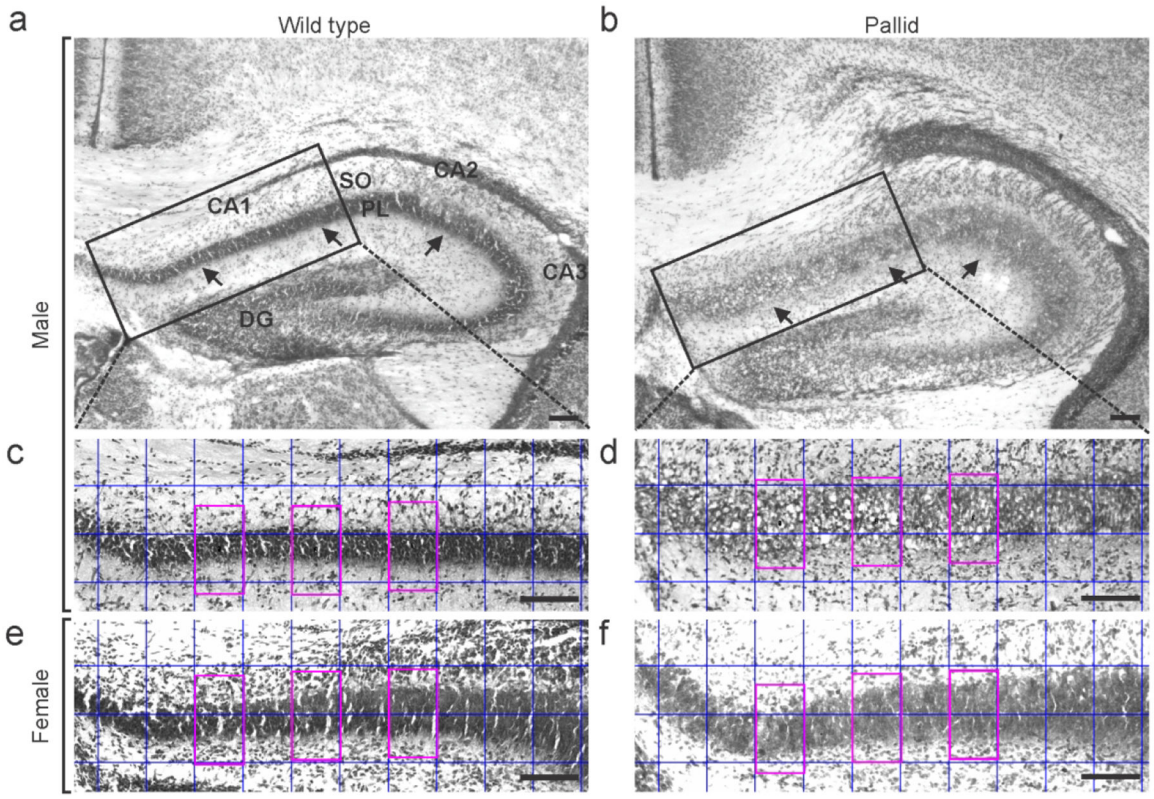

FIGURE 2.

Perturbed cellular organisation in the pyramidal cell layer of BLOC-1-deficient mice early postnatally. (a-f) Representative Nissl-stained sections of hippocampi from wild-type mice (a, c, e) and BLOC-1-deficient pallid mice (b, d, f), both males (a-d) and females (e, f), at postnatal day 1. CA, Cornu Ammonis; DG, dentate gyrus; PL, pyramidal layer; SO, stratum oriens. Arrows in (a) and (b) point at the pyramidal cell layer, which appears enlarged in pallid male mice (b). Black rectangles in (a) and (b) denote the regions shown at higher magnification in (c) and (d), respectively. Notice in the hippocampus from pallid males (b, d) the lack of a compact pyramidal cell layer in CA1 and their scattered presence in the stratum oriens. This phenotype was considerably less pronounced in the hippocampus of pallid females (f). Special care was taken to ensure that, prior to the staining, the slices from wild-type and pallid males and females were paired along the anterior-posterior axis. The magenta rectangles positioned on a blue grid were used to perform the profile plot analyses reported in Figure 3. Scale bars, 200 μm (a, b), and 100 μm (c-f).

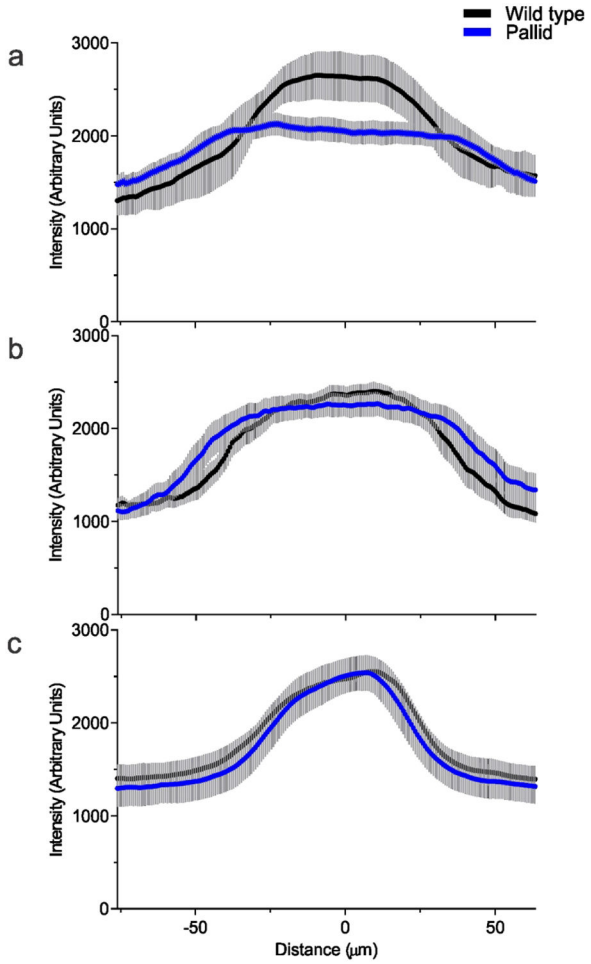

FIGURE 3.

Densitometric analysis of the cytoarchitecture of the pyramidal cell layer in the CA1 subfield from wild-type and BLOC-1-deficient hippocampi. (a-c) The relative staining intensity of Nissl-stained hippocampal sections was measured across the pyramidal cell layer of the CA1 area of wild-type and BLOC-1 deficient pallid mice at postnatal day (P)1 in males (a) and females (b), as well as at P45 in males (c), using a series of rectangular boxes (shown in Figure 2c–f in magenta colour) positioned on a fixed grid (shown in Figure 2c–f in blue colour) that were subjected to profile plot analysis by calculating average pixel intensity per row of pixels along the short axis as a function of position along the long axis of the rectangle. In every histological section, three rectangular boxes were analysed and averaged for each of the left and right hippocampi by two investigators masked to genotype, sex and age of the animal. The resulting profiles of 8–12 histological sections per animal were aligned (using polynomial curve fitting to automatically estimate the centre of the cell layer), and the aligned profiles averaged to obtain a single normalised profile per animal. The traces represent means ± SEM of five (a, b) or four (c) animals per genotype. Notice in (a) the relatively broad and flat peak of the normalised profile derived from pallid males at P1, as compared to that of age-matched wild-type males. Such anomaly was attenuated in pallid females at P1 (b) and undetectable in pallid males at P45, which resulted in a

normalised profile that was virtually indistinguishable from that of age-matched wild-type males (c).

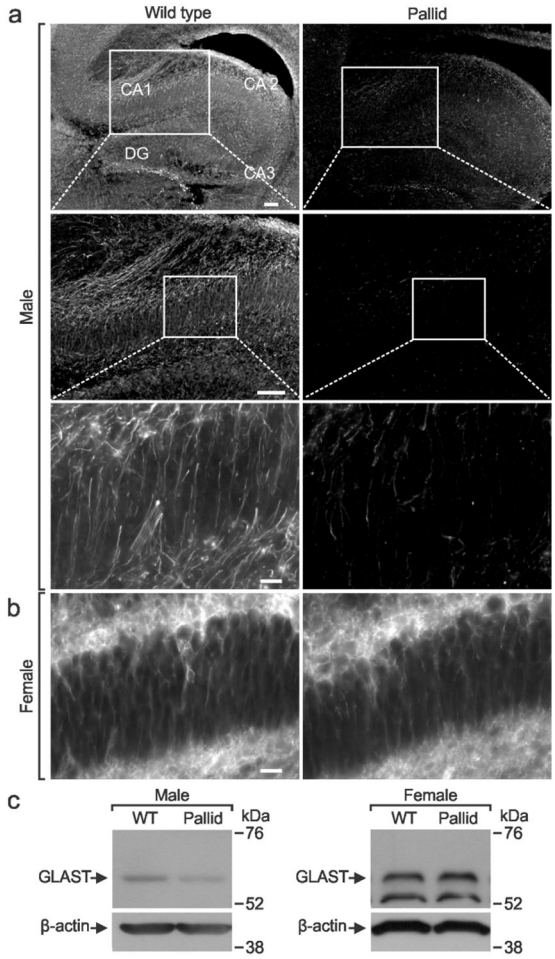

FIGURE 4.

Faulty radial glia scaffold in male BLOC-1-deficient hippocampi at postnatal day 1 (P1). (a) The paucity of fibres positive for the radial glia marker GLAST was remarkable throughout the hippocampus of BLOC-1-deficient pallid males at P1 as compared to sex- and age-matched wild-type controls, where well-arranged and defined GLAST-positive processes could be observed. For both genotypes, a representative immunostained section is shown at three progressively higher magnifications, with the white boxes in the top and middle images delineating the areas shown at higher magnification in the middle and bottom images, respectively. CA, Cornu Ammonis; DG, Dentate Gyrus. Scale bars, 100 μm (top and middle images) and 40 μm (bottom image). (b) Representative images of immunostained sections containing the CA1 area from wild-type and pallid females at P1, showing that the mutant females displayed GLAST-positive processes at a degree similar to age-matched wild-type females. Scale bar, 40 μm. (c) Representative western blotting of whole-tissue lysates of hippocampi from P1 mice. The total protein levels of GLAST were severely decreased in male, but not females, pallid hippocampi, as compared to sex- and age-matched wild-type (WT) mice. See Table 4 for the statistical analysis of the values obtained by quantitative densitometry of similar western blotting carried out for 4–5 animals per genotype and sex.

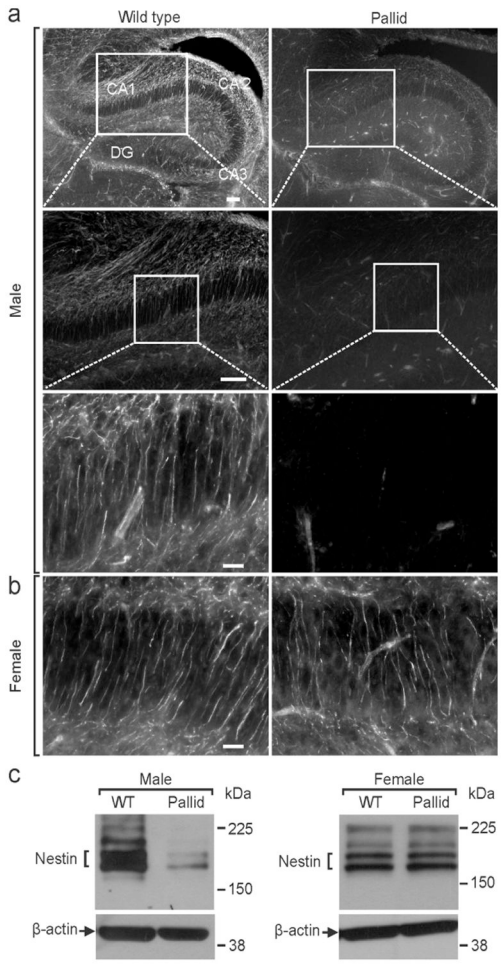

FIGURE 5.

Decreased expression of the neuroepithelial cell marker nestin in male BLOC-1-deficient hippocampi at postnatal day 1 (P1). (a) The scarcity of nestin immunostaining was observed in the hippocampus of BLOC-1-deficient pallid males at P1 as compared to sex- and age-matched wild-type controls. For both genotypes, a representative immunostained section is shown at three progressively higher magnifications, with the white boxes in the top and middle images delineating the areas shown at higher magnification in the middle and bottom images, respectively. CA, Cornu Ammonis; DG, Dentate Gyrus. Scale bars, 100 μm (top and middle images) and 40 μm (bottom image). (b) Representative images of immunostained sections containing the CA1 area from wild-type and pallid females at P1, showing that pallid females did not exhibit the striking decrease in nestin expression observed in pallid males. Scale bar, 40 μm. (c) Representative western blotting of whole-tissue lysates of hippocampi from P1 mice. The total protein levels of nestin were severely decreased in male, but not females, pallid hippocampi, as compared to sex- and age-matched wild-type (WT) controls. See Table 4 for the statistical analysis of the values obtained by quantitative densitometry of similar western blotting carried out for 4–5 animals per genotype and sex.

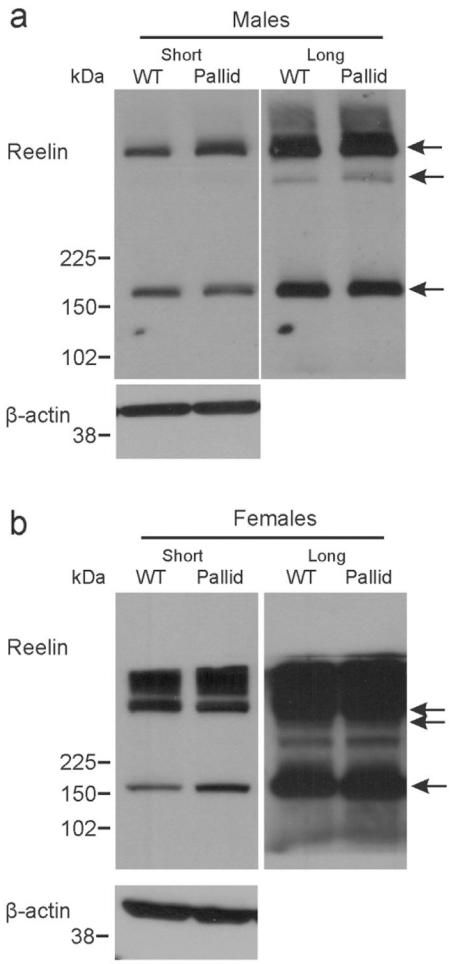

FIGURE 6.

Unchanged expression levels of the main reelin forms in BLOC-1-deficient mice hippocampi at postnatal day 1. Representative western blotting of whole-tissue lysates of hippocampi from male (a) and female (b) mice of the BLOC-1-deficient mutant strain pallid and sex- and age-matched wild-types (WT), showing the full-length reelin protein (400 kDa) as well as the main forms of reelin resulting from proteolytic cleavage. See Table 4 for the statistical analysis of the values obtained by quantitative densitometry of similar western blotting carried out for 4–5 animals per genotype and sex.

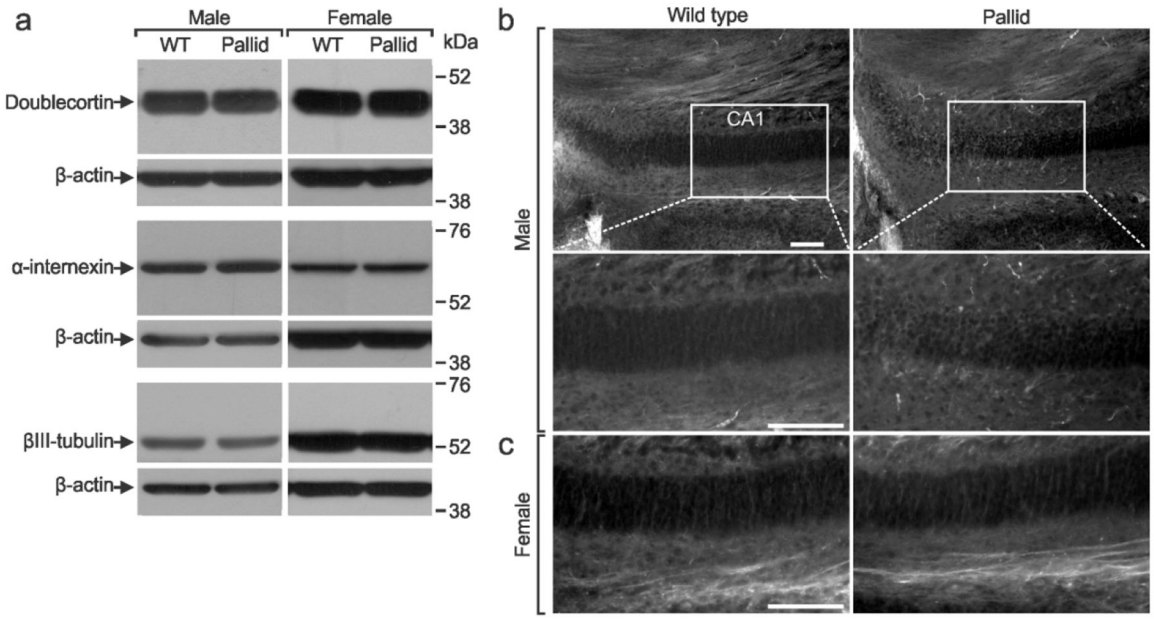

FIGURE 7.

Normal protein levels of neuroblast and neuronal markers but altered cytoarchitecture in the hippocampus of male BLOC-1-deficient mice at postnatal day 1 (P1). (a) Representative western blotting of whole-tissue lysates of hippocampi from P1 male and female mice of the BLOC-1-deficient mutant strain pallid and sex- and age-matched wild-type (WT) controls, showing no differences in the total protein levels of neuroblast (doublecortin) and neuronal (α-internexin and β-III tubulin) markers. See Table 4 for the statistical analysis of the values obtained by quantitative densitometry of similar western blotting carried out for 4–5 animals per genotype and sex. (b) Representative images of immunostained hippocampal sections containing the CA1 subfield of wild-type and pallid males at P1, showing the altered cell arrangement and expression pattern of α-internexin within the mutants' pyramidal cell layer. The white box in each image at the top delineates the areas shown at higher magnification in the bottom images. Scale bars, 100 μm. (c) The expression of α-internexin within the CA1 pyramidal cell layer of P1 pallid females was similar to that of sex- and age-matched wild-types. Scale bar, 100 μm.

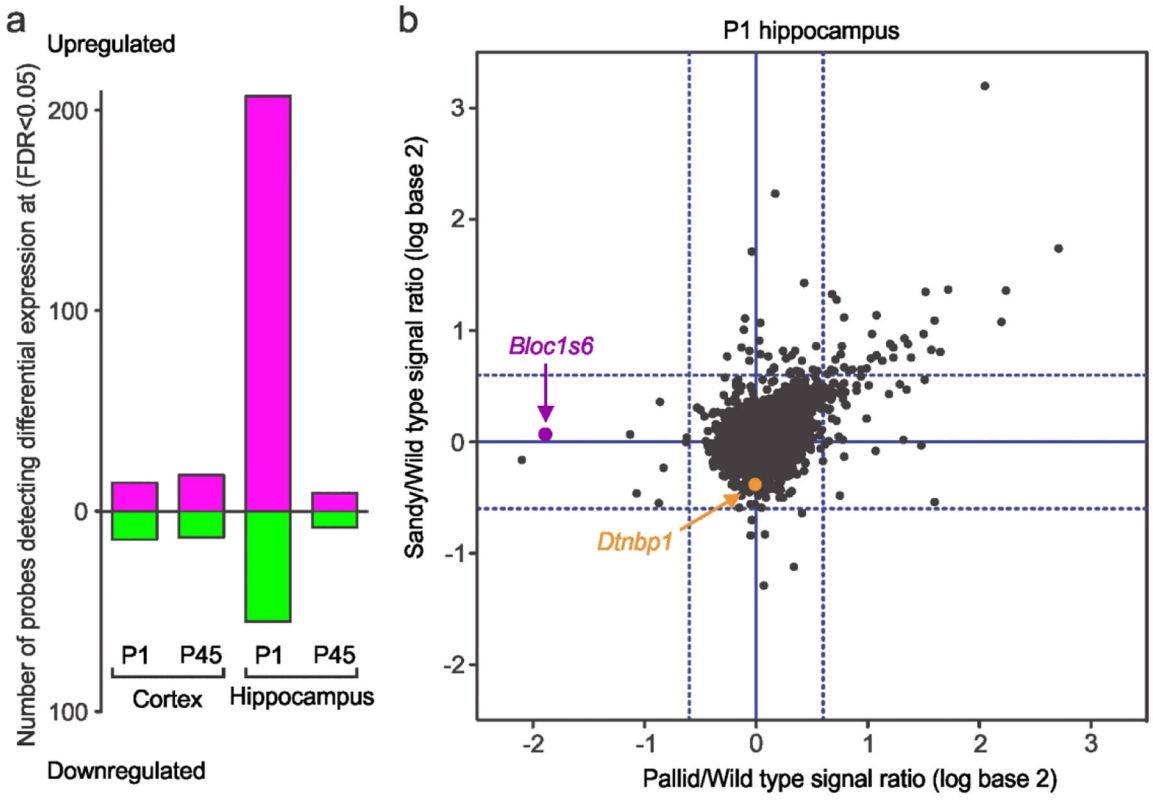

FIGURE 8.

Microarray-based transcriptomic analysis of hippocampus and cerebral cortex from BLOC-1-deficient mice at two developmental stages. (a) Schematic representation of the number of microarray probes (among those yielding reliable signal above noise level) that resulted in detection of genes whose expression was relatively increased (Upregulated, magenta bars), or decreased (Downregulated, green bars), in hippocampus and cerebral cortex from male pallid mice at postnatal day (P)1 or P45, as compared to the corresponding brain region from sex- and age-matched wild-type controls, at a false-discovery rate (FDR) of less than 0.05 (n=4 animals per group). Notice the relatively larger number of probes detecting differentially expressed genes in the hippocampus from P1 mice. (b) Correlation between the mutant/wild-type signal ratios obtained for two different BLOC-1-deficient strains, pallid and sandy, by microarray analysis of total RNA isolated from hippocampi dissected from mutant and wild-type male mice at P1 (n=4 animals per group). Each dot represents a probe yielding a relatively strong signal (defined as within the top third of all probe signals from the microarray), with the value on the *x* axis representing the logarithm in base 2 of the ratio between the average signals obtained for 4 pallid and 4 sex- and age-matched wild-type samples, and the value on the *y* axis representing the logarithm in base 2 of the ratio between the average signals obtained for 4 sandy and 4 sex- and age-matched wild-type samples. Solid blue lines indicate no change in transcript expression between pallid (vertical line) or sandy (horizontal line) and their corresponding wild-type controls, and dashed blue lines denote mutant/wild-type signal ratios corresponding to a factor of 1.5 (50% increase, or decrease to two-thirds, relatively to wild-type levels). Notice that the transcript from the *Bloc1s6* gene, which is mutated in pallid mice, was decreased in pallid

mice but not in sandy mice. Conversely, the transcript from the *Dtnbp1* gene, which is mutated in sandy mice, was slightly decreased in sandy mice but apparently not in pallid mice. Notice also that a small subset of probes detected transcripts that were upregulated by a factor larger than 1.5 in both pallid and sandy mice (upper right quadrant of the figure).

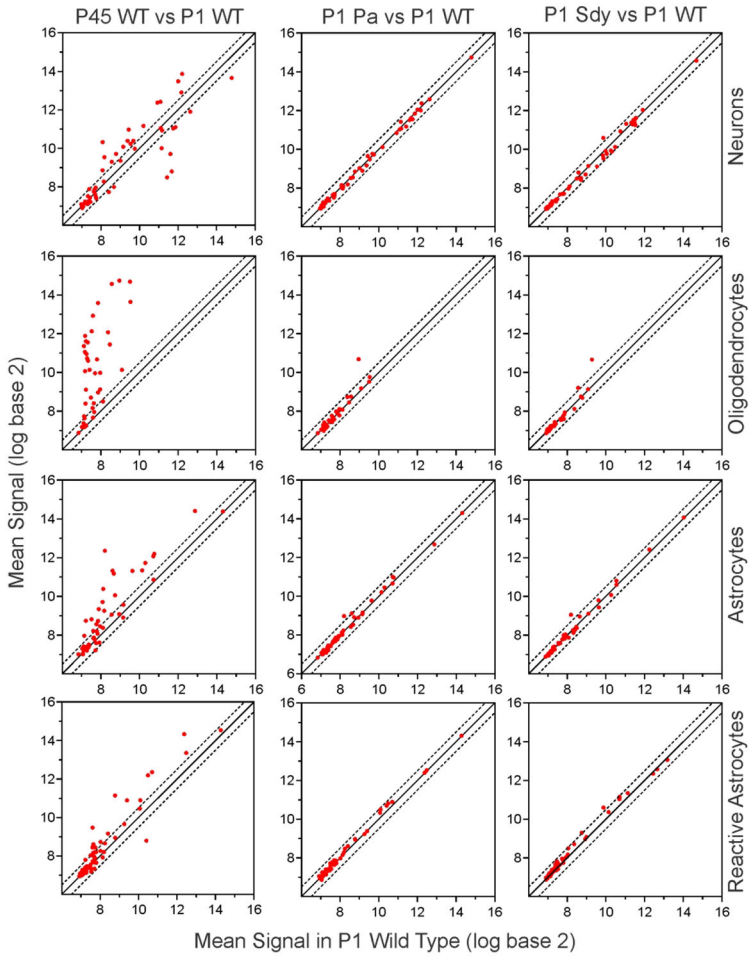

FIGURE 9.

The transcriptomic signature observed in the hippocampus from BLOC-1-deficient mice at postnatal day (P)1 was not secondary to changes in the populations of glial cell subtypes. The average signals obtained for microarray probes detecting transcripts that are considered cell-type-specific markers of neurons, oligodendrocytes and astrocytes (Chaoy et al., 2008) or markers of reactive astrocytes (lipopolysaccharide (LPS)-injected mice; Zamanian et al., 2012) in hippocampi from male wild-type (WT) mice at P1 were compared against those in hippocampi from male wild-type mice at P45 (left column of graphs), in hippocampi from male BLOC-1-deficient pallid (Pa) mice at P1 (middle column of graphs), and in hippocampi from male BLOC-1-deficient sandy (Sdy) mice at P1 (right column of graphs). In all graphs, each data point corresponds to a marker transcript, with the value on each axis representing the logarithm in base 2 of the average of signals obtained for 4 animals per group. In each graph, a solid diagonal line denotes no difference in expression levels, while the dashed diagonal lines indicate changes in transcript levels (increase or decrease relatively to wild type at P1) by a factor of 1.5. While a large number of marker transcripts was differentially expressed in wild-type hippocampi between P1 and P45, in part reflecting normal changes in the population of different cell types (such as proliferation and maturation

of oligodendrocytes and astrocytes) during postnatal brain development, very few of these markers were deemed to be differentially expressed in mutant hippocampi at P1.

Table 1.

Antibodies used in the present study.

Target	Clone	Host Species	Immunogen	Dilutions used		Cat. Number	Company	RRID
Monoclonals				WB	IHC			
β-actin	AC-15	Mouse	Slightly modified β-actin N-terminal peptide (Ac-DDDIAALVIDNGSGK) conjugated to KLH.	1:10,000	--	A5441	Sigma-Aldrich	AB_476744
GLAST	8C11.1	Mouse	GST-tagged recombinant protein corresponding to the extracellular domain of human GLAST.	1:1,000	1:250	MABN794	Millipore	AB_2811303.
Nestin	Rat401	Mouse	Rat (E15) spinal cord extracts.	1:1,000	1:100	556309	BD Biosciences	AB_396354
Reelin	142	Mouse	Recombinant reelin amino acids 40–189.	1:1,000	--	MAB5366	Millipore	AB_2285132
Polyclonals								
α-Internexin		Rabbit	Full length recombinant rat α-internexin fused to *E. coli* Trp E.	1:500	1:200	AB5354	Millipore	AB_91800
β-III tubulin	Tuj1	Rabbit	Microtubules derived from rat brain.	1:10,000	1:200	PRB-435P	Covance	AB_2564645
Doublecortin		Rabbit	A synthetic peptide corresponding to human doublecortin.	1:1,000	1:300	#4604	Cell Signaling	AB_561007
GLAST		Guinea Pig	Rat c-terminal peptide sequence: QLIAQDNEPEKPVADSETKM	1:1,000	1:250	AB1782	Millipore	AB_90959

WB: western blot; IHC: immunohistochemistry

J Neurosci Res. Author manuscript; available in PMC 2021 July 01.

Table 2.

Two-way analysis of variance (ANOVA) analysis of the data shown in Figure 1. Degrees of freedom are reported within parentheses, alpha=0.05. P: postnatal day; n: number of animals per group. Bold type indicates statistical significance.

Panels	**Wild type (n)**		**pallid (n)**		**Genotype**	**Sex**	**Interaction [sex x genotype]**
	males	females	males	females			
a: Brain weight	25	13	28	21	$\mathbf{F_{(1,83)}=6.01;\ P=0.0163}$	$F_{(1,83)}=1.95;\ P=0.1659$	$F_{(1,83)}=1.49;\ P=0.2258$
b: Body weight	14	13	19	21	$F_{(1,63)}=2.79\ P=0.0999$	$F_{(1,63)}=0.12;\ P=0.7254$	$F_{(1,63)}=0.55;\ P=0.4607$
c: Ratio	14	13	19	21	$\mathbf{F_{(1,63)}=14.4;\ P=0.0003}$	$F_{(1,63)}=0.01;\ P=0.9136$	$F_{(1,63)}=0.92;\ P=0.3412$
d					Genotype	Age	Interaction [genotype x age]
P1	22		23		$\mathbf{F_{(1,76)}=9.57;\ P=0.0028}$	$\mathbf{F_{(2,76)}=6916;\ P<0.0001}$	$F_{(2,76)}=1.71;\ P=0.1872$
P14	13		11				
P45	7		6				

Table 3.

Gross morphometrical analysis of the cerebral cortex and hippocampus reveals no differences between wild-type and pallid male mice. The thickness of the cerebral cortex, layers 1 through 6, was measured as a continuous line drawn from the most external margin of layer 1 up to the limit with the corpus callosum. The fimbria was not included in the measurements of the total area or perimeter of the hippocampus. Two-way analysis of variance (ANOVA) showed no significant effect of genotype. Measurements were performed by two independent observers masked to the genotype and age in male wild-type and pallid mice at postnatal day (P)1 and P45, since females did not show significant differences in other assessments. Results are shown as the mean ± SEM of 5 P1 mice per genotype and 4 P45 mice per genotype. Degrees of freedom are reported within parentheses; alpha=0.05.

		Rostral Cerebral Cortex: Thickness (μm)	**Genotype**	**Age**	**Interaction Effect (genotype x age)**
P1	Wild type	2229 ± 92.9	$F_{(1,14)}$=2.02; P=0.177	$F_{(1,14)}$=520; P<0.0001	$F_{(1,14)}$=0.23; P=0.635
	pallid	2072 ± 81.5			
P45	Wild type	4060 ± 72.5			
	pallid	3983 ± 64.9			
		Caudal Cerebral Cortex: Thickness (μm)			
P1	Wild type	1850 ± 66.2	$F_{(1,14)}$=0.25; P=0.625	$F_{(1,14)}$=298; P<0.0001	$F_{(1,14)}$=1.13; P=0.305
	pallid	1815 ± 31.3			
P45	Wild type	2838 ± 89.7			
	pallid	2933 ± 47.3			
		Hippocampus: Outer Border (mm)			
P1	Wild type	12.40 ± 0.33	$F_{(1,14)}$=0.68; P=0.421	$F_{(1,14)}$=699; P<0.0001	$F_{(1,14)}$=0.47; P=0.504
	pallid	12.03 ± 0.13			
P45	Wild type	18.64 ± 0.21			
	pallid	18.61 ± 0.22			
		Hippocampus: Sectional Area (mm^2)			
P1	Wild type	7.582 ± 0.53	$F_{(1,14)}$=0.07; P=0.788	$F_{(1,14)}$=841; P<0.0001	$F_{(1,14)}$=3.18; P=0.096
	pallid	8.213 ± 0.14			
P45	Wild type	20.45 ± 0.53			
	pallid	19.59 ± 0.34			

Table 4.

Statistical table of the western blot analyses of neural cell markers and reelin in wild-type and pallid hippocampi at postnatal day 1. Absence of BLOC-1 significantly affects the expression levels of markers for radial glial cells in male hippocampi, but not in females, as compared to wild-type controls. Values derived from densitometric analysis were corrected for background, normalised to β-actin, and expressed as a ratio of the normalised value obtained for each pair of pallid and wild-type hippocampi, which were processed and analysed in parallel. Results are reported as the means ± SEM of 4–5 pairs of wild-type and pallid animals per sex. One-sample *t* test against a theoretical value of 1, Alpha=0.05. Bold type indicates statistical significance.

		Relative Protein Expression levels (mutant-to-wild-type ratio)			
Figure	**Markers**	**Males**	**One-sample *t* test**	**Females**	**One Sample *t* test**
4c	GLAST	**0.64 ± 0.05**	***t*(4)=6.853; *P*=0.0024**	1.09 ± 0.14	*t*(4)=0.663; *P*=0.5435
5c	Nestin	**0.54 ± 0.15**	***t*(4)=3.054; *P*=0.0379**	0.92 ± 0.11	*t*(4)=0.680; *P*=0.5332
6	Reelin				
	400 kDa	1.07 ± 0.14	*t*(3)=0.548; *P*=0.6220	1.18 ± 0.44	*t*(4)=0.399; *P*=0.7097
	300 kDa	0.88 ± 0.28	*t*(3)=0.416; *P*=0.7050	0.94 ± 0.22	*t*(4)=0.262; *P*=0.8065
	180 kDa	0.95 ± 0.25	*t*(3)=0.199; *P*=0.8544	1.14 ± 0.16	*t*(4)=0.875; *P*=0.4311
7a	Doublecortin	0.96 ± 0.02	*t*(4)=1.343; *P*=0.2505	0.94 ± 0.07	*t*(4)=0.872; *P*=0.4325
7a	α-internexin	1.04 ± 0.04	*t*(4)=0.923; *P*=0.4082	1.08 ± 0.09	*t*(4)=0.819; *P*=0.4586
7a	β-III tubulin	0.99 ± 0.07	*t*(3)=0.157; *P*=0.8852	1.00 ± 0.07	*t*(4)=0.055; *P*=0.9577

Table 5.

Genes upregulated in hippocampi from BLOC-1-deficient mice at postnatal day (P)1 as inferred from microarray-based transcriptomic analyses of homozygous pallid and sandy mutant mice. The list was derived from the analysis shown in Figure 8b and consists of genes whose transcripts were upregulated in both BLOC-1-deficient mutants, pallid (Pa) and sandy (Sdy), by a factor greater than 1.5 relative to their corresponding wild-type (WT) controls (n=4 animals for each group). Three genes were detected by more than one probe in the microarray, with comparable results. Listed also are the average signal ratios obtained by comparing hippocampi from WT mice at P1 and P45 as well as from Pa and WT mice at P45.

Mouse gene	Human ortholog				Average signal ratio			
		Official full name	Transcript ID	Probe ID	Pa/WT (P1)	Sdy/WT (P1)	P45/P1 (WT)	Pa/WT (P45)
Acta2	*ACTA2*	Actin, alpha 2, smooth muscle, aorta	NM_007392	ILMN_218281	1.8	1.6	6.6	0.9
Aebp1	*AEBP1*	AE binding protein 1	NM_009636	ILMN_2873822	2.0	1.6	2.5	0.9
Apod	*APOD*	apolipoprotein D	NM_007470	ILMN_2668927	1.6	2.4	6.7	1.1
Aqp1	*AQP1*	Aquaporin 1	NM_007472	ILMN_2756486	4.7	2.6	3.9	1.5
				ILMN_2980661	2.1	2.0	1.8	1.3
Cldn11	*CLDN11*	Claudin 11	NM_008770	ILMN_1246139	3.3	2.6	54.9	1.0
Clic6	*CLIC6*	Chloride intracellular channel 6	NM_172469	ILMN_2667635	6.5	3.3	15.3	1.3
Col6a1	*COL6A1*	collagen, type VI, alpha 1	NM_009933	ILMN_2768087	1.6	1.6	2.6	0.9
Defb11	—*	Defensin beta 11	NM_139221	ILMN_2599861	4.6	2.1	5.4	1.1
Ecrg4	*ECRG4*	ECRG4 augurin precursor	NM_024283	ILMN_1249000	2.5	1.9	4.4	1.1
Enpp2	*ENPP2*	Ectonucleotide pyrophosphatase/phosphodiesterase 2	NM_015744	ILMN_2954474	2.6	1.7	18.4	1.1
Folr1	*FOLR1*	Folate receptor 1 (adult)	NM_008034	ILMN_2707541	2.3	1.8	4.2	1.5
				ILMN_3000679	2.2	1.7	2.7	1.4
Gjb6	*GJB6*	Gap junction protein, beta 6	NM_008128	ILMN_214830	1.7	1.8	17.8	1.1
Gpc3	*GPC3*	Glypican 3	NM_016697	ILMN_2719973	2.1	1.7	1.3	1.0
				ILMN_2832979	2.3	1.8	1.3	0.9
H19	*H19*	H19, imprinted maternally expressed transcript	NR 001592	ILMN_2906728	1.6	2.5	0.5	1.0
H1f2	*H1–2*	H1.2 linker histone, cluster member	NM_015786	ILMN_2855315	1.6	1.6	3.6	0.9
Igf2	*IGF2*	Insulin-like growth factor 2	NM_010514	ILMN_2597769	2.0	1.7	1.9	1.1
Kcne2	*KCNE2*	Potassium voltage-gated channel, Isk-related subfamily, gene 2	NM_134110	ILMN_2794237	3.0	1.8	3.9	1.2
Mgp	*MGP*	Matrix Gla protein	NM_008597	ILMN_215984	1.7	2.2	7.8	1.0

Mouse gene	Human ortholog				Average signal ratio			
		Official full name	Transcript ID	Probe ID	Pa/WT (P1)	Sdy/WT (P1)	P45/P1 (WT)	Pa/WT (P45)
Mia	*MIA*	Melanoma inhibitory activity	NM_019394	ILMN_2880657	1.9	1.6	1.0	0.9
Msx1	*MSX1*	Msh homeobox 1	NM_010835	ILMN_1246173	1.7	1.6	2.7	1.0
Ogn	*OGN*	Osteoglycin	NM_008760	ILMN_2859613	2.3	1.8	3.0	1.0
Otx2	*OTX2*	Orthodenticle homeobox 2	NM_144841	ILMN_2691752	3.1	1.8	3.1	1.2
Rbm47	*RBM47*	RNA binding motif protein 47	NM_178446	ILMN_218273	2.6	1.8	3.5	1.2
Ptdgs	*PTDGS*	Prostaglandin D2 synthase (brain)	NM_008963	ILMN_1248316	2.9	2.5	17.4	1.0
Slc6a13	*SLC6a13*	Solute carrier family 6 (neurotransmitter transporter, GABA), member 13	NM_144512	ILMN_1212645	2.1	2.2	1.3	0.8
Slc13a4	*SLC13A4*	Solute carrier family 13 (sodium/sulfate symporters), member 4	NM_172892	ILMN_2827072	3.0	2.1	7.1	1.0
Sostdc1	*SOSTDC1*	Sclerostin domain containing 1	NM_025312	ILMN_2642800	2.8	2.0	4.3	1.5
Tgfbi	*TGFBI*	Transforming growth factor, beta induced	NM_009369	ILMN_2834379	1.8	1.6	1.8	1.1
Ttr	*TTR*	Transthyretin	NM_013697	ILMN_2443330	4.1	9.2	4.4	1.1
Vtn	*VTN*	vitronectin	NM_011707	ILMN_1234111	1.7	1.7	3.0	0.9
Zic1	*ZIC1*	Zinc finger protein of the cerebellum 1	NM_009573	LMN_2491186	2.3	1.7	1.5	0.8

*No recognisable human ortholog.

Table 6.

Validation by quantitative real-time polymerase chain reaction (qPCR) of a subset of the genes whose expression was increased in hippocampi from BLOC-1-deficient mice at postnatal day (P)1 as judged by microarray analysis. The relative expression levels of genes selected from those listed in Table 5 were determined by qPCR in sets of hippocampi from wild-type (WT) mice (n=7–9) and BLOC-1-deficient pallid mice (n=10–11) that were independent from those used for the microarray analyses reported in Figure 8 and Table 5. The expression levels of two housekeeping genes, *Ppia* and *Ubc*, were analysed in the same samples. For each gene listed in the table (including *Ubc*), average values from 3 technical replicates per sample were normalised to those obtained for *Ppia* in the same sample, and the transcript levels in the mutant samples were expressed as means ± SEM relative to the mean value obtained for the WT samples. As expected, the relative expression level of the housekeeping gene *Ubc*, normalised to *Ppia*, was indistinguishable from the theoretical value of 1. Similar results were obtained when the values per sample for each gene were normalised to the geometric mean of those for the two housekeeping genes in the same sample. Mann-Whitney test, alpha=0.05. Bold type indicates statistical significance.

Gene	Gene ID	Catalog No	Expression levels (relative to WT)	Mann-Whitney test
Ubc	22190	QT00245189	0.99 ± 0.04	*U*=41; *P*=0.3901
Aqp1	11826	QT00109242	**1.57 ± 0.19**	***U*=14; *P*=0.0215**
Cldn11	18417	QT00104195	**1.87 ± 0.25**	***U*=19; *P*=0.0100**
Gpc3	14734	QT00118790	1.17 ± 0.15	*U*=40; *P*=0.2514
Igf2	16002	QT00109879	**1.54 ± 0.16**	***U*=16; *P*=0.0048**
Msx1	17701	QT01661821	**1.35 ± 0.12**	***U*=20; *P*=0.0253**
Ptgds	19215	QT00098049	**6.06 ± 2.25**	***U*=16; *P*=0.0102**
Ttr	22139	QT00107485	1.67 ± 0.51	*U*=28; *P*=0.1030

Table 7.

Top enriched biological functions inferred by Gene Set Enrichment Analysis (GSEA) of the results from microarray analyses of hippocampi from two BLOC-1-deficient mutants, pallid and sandy, and their corresponding wild-type (WT) controls. Datasets comprising the relative signals obtained in each mutant and its WT control for all microarray probes yielding relatively strong signals (defined as within the top third of all probe signals in at least one sample) were subjected to GSEA using standard parameters (5–2000 genes per category, Benjamini-Hochberg procedure to control for multiple comparison). Gene ontology (GO) categories that were significant at a false discovery rate (FDR) of less than 0.05 in both datasets are listed. NES, normalised enrichment score.

		Pallid vs WT		Sandy vs WT	
GO Number	**GO Name**	**NES**	**FDR**	**NES**	**FDR**
0048568	Embryonic organ development	2.03	0.0125	1.97	0.0394
0043062	Extracellular structure organization	2.01	0.0112	2.11	0.0173
0007178	Transmembrane receptor protein serine/threonine kinase signalling pathway	2.01	0.0121	1.99	0.0486
0090287	Regulation of cellular response to growth factor stimulus	1.99	0.0133	1.98	0.0445
0009611	Response to wounding	1.98	0.0133	1.94	0.0413
0001655	Urogenital system development	1.98	0.0129	1.93	0.0429
0001763	Morphogenesis of a branching structure	1.96	0.0149	2.13	0.0276
0048771	Tissue remodelling	1.93	0.0193	1.94	0.0451